OPTICAL AND DIGITAL METHODS FOR THE ANALYSIS OF MICROSCOPIC TISSUE SECTIONS

by

A.R.Eastgate, B.Eng., M.Sc.(Qual)

Submitted in partial fulfilment
of the requirements for the degree
of Master of Science.

graduation 1986

UNIVERSITY OF TASMANIA
HOBART December 1985

I declare that this thesis contains no material which has been accepted for the award of any other degree or diploma in any university, and that, to the best of my knowledge and belief, this thesis contains no copy or paraphrase of material previously published or written by any other person, except where due reference is made in the text of the thesis.

(A.R.Eastgate)

December 1985.

CONTENTS

ABSTRACT

This thesis presents optical and computer-based methods for the analysis of microscope specimens that are in the form of thin sections that have been mounted on standard glass slides.

Three methods are discussed whereby image and photometric information can be obtained - television scanning, microphotometric scanning and micro-spectrophotometry. The limitations of these methods are analysed and some representative results are given.

The thresholding of digital image data with the assistance of neighbourhood operators is examined, with particular reference to the Laplacian and Gradient operators.

A method for the statistical analysis of tissue-section textures is presented and is shown to be applicable the discrimination of two pathological classes of human prostate tissue. The effectiveness of the method is evaluated by the use of a computed Mahalanobis distance for the various statistics used.

Chapter 1 : Introduction

The task of image analysis is one that pervades our daily lives so thoroughly that we are scarcely, if ever, aware of the range and sophistication of the intellectual processes constantly at work behind those obvious witnesses to our visual activity, the eyes. Decisions about colour, texture, shape and spatial disposition are continually being made in only fractions of seconds, with the least conscious direction required; it is all, as we say, automatic.

In terms of that quantum of the information world, the bit, the number of quanta required to fully describe a typical outdoor scene down to the resolution of the human eye is almost astronomical. Billions of constantly-changing bits would be required for such a scene. The first task of visual perception is to determine what is relevant and to reduce this information surplus to manageable levels.

In the detection and recording of microscopic detail, which is the subject of the first parts of this study, reduction of the information in the image of the specimen will be shown to be an inevitable consequence of the nature of the sampling processes used : scanning microphotometry and television scanning. The nature of this information-loss is discussed.

With many microscope specimens the final result of the analysis can be expressed in surprisingly few words. Often it is only a proportion that is sought, such as "13.4% Diopside", for the geologist, or a choice between two alternatives, such as a Cancer/Benign diagnosis for the clinician.

Even more surprising is the extent of the information about the specimen which would constitute a sufficient minimum for a satisfactory analysis to be made. The selection of this minimum quantity is something that is not addressed in this study; it relates to the ability of visual

automata to "understand" a scene, something which is still being actively researched. Hall (1.1) gives a summary of what has been achieved in this field; he divides scene comprehension into four tasks: segmentation, region-description, relational description and object formation. Segmentation requires an understanding of spatial relationships in the general case, as does the formation of relational descriptions such as "behind" or "inside of". The region-description task for the case of two-dimensional microscope images and the derivation of sensible conclusions about these images , the object formation task, is shown to be achievable with a microcomputer.

A review of the image-processing capabilities of a general-purpose microcomputer has been given recently by Russ and Russ (1.2). The system they describe performs many operations on images in a shorter time than much larger and more expensive computers. In this study the reduction of information present in the microscope image is pursued even further, to the ultimate level of a single proportion or a single diagnosis.

Chapter 2 : Scanning Microphotometry

A microphotometer can form scanned images of microscope specimens when the microscope stage is motor-driven and can translate the specimens under the objective lens in a programmed pattern. The images thus formed are slow to collect but usually have a high signal to noise ratio. The primary requirement in such scanning may often be the collection of statistical information about inhomogeneous specimens, in which case image fidelity may be sacrificed for an increase in speed. Sandritter and Kiefer (2.1) give a comprehensive review of microphotometer instrumentation and methodology, as does Zimmer (2.2); only the advent of the powerful and inexpensive range of modern microcomputers in the last decade requires a deeper investigation of the microphotometer's potential, particularly in the area of digital image acquisition and analysis.

The Leitz MPV2 microphotometer has two motorized stepping-stages, with 0.5 m and 10 m. step sizes. An interface between the MPV2 and its instrument-computer, an Acorn BBC Micro, has been constructed by the author to match the computer's parallel-port TTL-level signals to the inputs of the stepping-stage drive circuitry and to match the output of the MPV2 photometer-amplifier to the input of the computer's analogue-to-digital converter (ADC). Thus there are two restrictions upon scanning speed : the minimum conversion-time of the ADC is 4 milliseconds and the minimum time required for each step of the motorized stage is approximately the same. Allowing a 2 millisecond 'overhead' per sample-point for direction-changes and other system delays, the minimum time for a typical scan of 16,384 points is just under three minutes; experience has shown this to be an acceptable figure for most applications to date.

Obtaining image-fidelity is mainly a matter of keeping illumination as strong as possible and ensuring that the stepping-stage does not stall or miss steps. Obtaining repeatable and meaningful results requires much more : Specimens for microphotometry should be prepared with the highest standards of

cleanliness, the luminous-field and measuring stops should be carefully adjusted for relative size and concentricity, and the instrument must be free of zero-error (due to dark current, for example) and drift. Under the best possible conditions a sample as small as 10,000 molecules should be able to be detected (2.2). A comprehensive description of the microphotometer and its method of operation has been given in an earlier report (2.3).

The theory of scanned image formation has been extended greatly since Mertz and Gray published their pioneering paper on television images in 1934 (2.4). Fourier analysis of the sampling process has shown that a two-dimensional sampling of a band-limited image f(x,y) can completely represent the image if samples are taken with separations no greater than $\Delta x = \frac{1}{2W_u}$ and $\Delta y = \frac{1}{2W_v}$, where W_u and W_v are the spatial frequency limits of the image in the x and y directions (2.5).

In the scanning microphotometer the light-sampling is performed by a sampling-aperture of finite size and is markedly affected by diffraction for diameters less than one micron. Usually the aperture is square or circular and ranges in diameter from 0.5μm. to 100μm. In analysis of this sampling the filtering effect of the aperture can be described by its point-spread function (PSF), h(x,y). The spatial frequency limits in the original image are generally those imposed by the microscope optics and are at least an order of magnitude beyond the representation limits imposed by Shannon's sampling theorem above ($\sim 20\mu$m.) when the usual (10μm.) stepping-stage is in operation. Thus the choice of sampling-aperture size must be made mainly with regard to the size of the step between samples and the need to make a compromise between adequate light throughput to the photometer and the avoidance of blur (when the sampling-aperture diameter is too large).

Figure 2-1 below shows a one-dimensional idealised image f(x-u) that has a step dislocation at x=u. If it is assumed that diffraction is absent and that the aperture has the characteristic shown, where s is the

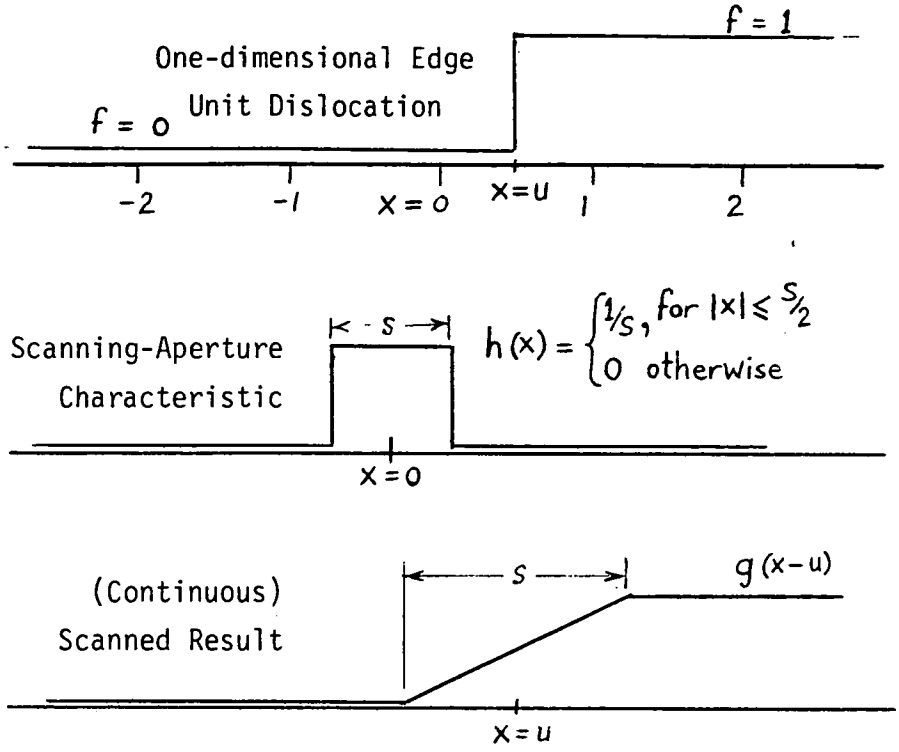

Figure 2-1 : Scanning Over An Idealised Dislocation.

instantaneous field of view (IFOV) in units of sample interval, then the resulting scanned image is a ramp of width s and is centred at x=u, the convolution of h(x) and f(x-u) :

$$g(x-u) = h(x) \ast f(x-u)$$

$$= \begin{cases} 1 & \text{for } x > [u + (s/2)] \\ \frac{x-u}{s} + \frac{1}{2} & \text{for } |x-u| \leq s/2 \\ 0 & \text{for } x < [u - (s/2)] \end{cases}$$

Thus the error resulting from such a sampling can be calculated as :

$$(\text{error})^2 = \int_{-\infty}^{\infty} [f(x-u) - g(x-u)]^2 dx$$

$$= \int_{u-s/2}^{u+s/2} f(x-u) - \left(\frac{x-u}{s}\right)^2 dx$$

$$= \int_{u-s/2}^{u} \left(\frac{x-u}{s}\right)^2 dx + \int \left(1 - \frac{(x-u)}{s}\right)^2 dx$$

$$\text{error} = s/12$$

This result indicates that, in the absence of significant

diffraction effects and when the sampling intervals are very small, the sampling aperture should be kept as small as possible. Light throughput is always a limiting factor however and aberrations in the objective lens are thought to modify the PSF of the system slightly. Aberration has been modelled by Goodman (2.6) as a phase-shifting plate inserted in the aperture and whose sole effect is to produce phase distortions within the pass-band of the system. The effect of diffraction for the normal range of aperture-sizes can be seen to be quite small from the relationship plotted in Fig.2-2 below. Deviation from linearity in these plots is more due to inaccuracy in manual setting of the aperture-size than anything else.

A general analysis of image degradation due to aliasing and blur in discrete data obtained with optical scanners has been presented by Huck et al.,(2.7). The optimisation of shape for apertures of constant transmittance has been dealt with by Katzberg et al.(2.8) and it was shown that a diamond-shaped aperture combined with an electronic low-pass filter reduces aliasing to the levels obtained with a graded-transmittance (Gaussian) aperture. The square and circular apertures used in the MPV2 microphotometer are thus inferior in this respect; their spatial-frequency responses have significant side-lobes, so that the resulting admission of high spatial frequency image content is best reduced by decreasing the sampling intervals or increasing aperture diameters. An analysis of this problem follows.

If we denote the effective aperture-width by γ and the sample-steps in the two orthogonal directions by X and Y, then the sample-intervals can be expressed as $s_x = X/\gamma$ and $s_y = Y/\gamma$. Normally $s_x = s_y$ for the micro-photometer scanning process, and $X = Y = 10\mu m$. For most image-scanning systems $0.5 \leq s \leq 1.0$ and there is still controversy as to which value of s is generally 'best'. Huck et al. (2.7) computed the relative amounts of blur and aliasing produced by a circular aperture of constant transmittance (and two other types) as s was varied over the range indicated above, by looking

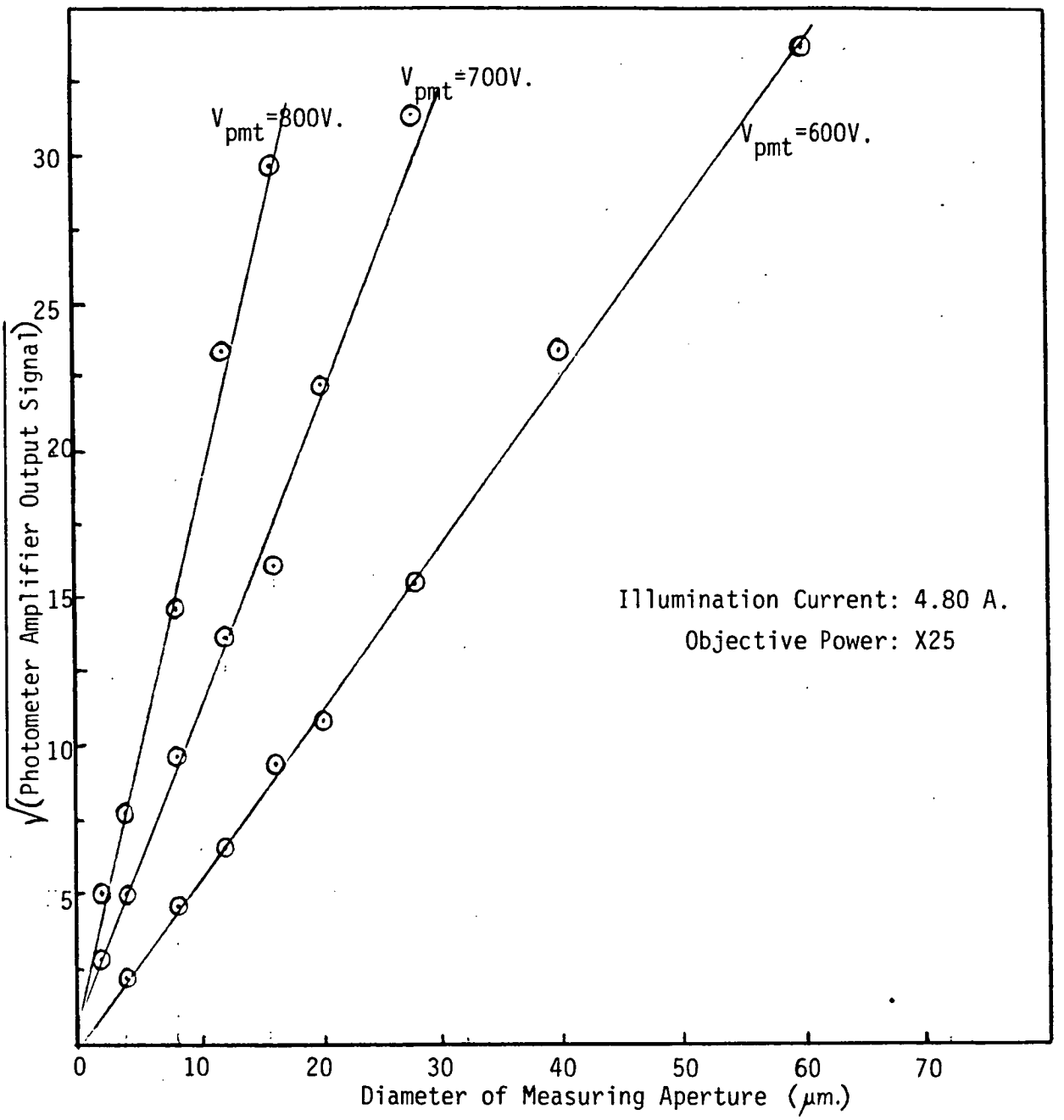

Fig.2-2: Relationship between Photometer Signal and Size of Measuring Aperture.

at the scanned image formation of a random field of two-dimensional pulses whose widths r obey a Poisson probability density function with expected mean width μ_r and whose magnitudes obey a Gaussian probability density function with variance σ_L^2. The Wiener spectrum of such a field is :

$$\Phi(\nu, w) = \frac{2\pi \mu_r^2 \sigma_L^2}{1+(2\pi\mu_r\rho)} \quad , \text{ where } \rho^2 = \nu^2 + w^2$$

and its autocorrelation function is :

$$\phi(r) = \sigma_L^2 \exp(\frac{-r}{\mu_r}) \quad , \text{ where } r^2 = x^2 + y^2.$$

This random field is similar to a wide range of scenes, including well-focussed microscope images of natural tissue sections. A sensor, the PMT with its sampling aperture in the case of the microphotometer, converts this continuous random field L(x,y) into the sampled form s(x,y;X,Y) that is stored in the memory of the instrument computer as discrete values. Thus the processes to be analysed are described by the equations :

$$s(x,y) = L(x,y) \ast h(x,y) \quad , \text{ a convolution,}$$

$$\text{and} \quad s(x,y;X,Y) = s(x,y).\text{comb}(\frac{x}{X}, \frac{y}{Y}) \ .$$

The Fourier transform of the sampling equation above can be otherwise expressed as :

$$\hat{s}(\nu,w;X,Y) = \sum_{m=-\infty}^{\infty} \sum_{n=-\infty}^{\infty} \hat{s}(\nu - \frac{m}{X}, w - \frac{n}{Y})$$

$$= \hat{s}(\nu,w) + \hat{s}_a(\nu,w;X,Y) \ ,$$

where $\hat{s}(\nu,w)$ is the continuous (unsampled) component and $\hat{s}_a(\nu,w;X,Y)$ represents the sideband components generated by sampling. Halyo and Stallman (2.9) have shown that the spectral components in the reconstructed signal r(x,y) due to $\hat{s}(\nu,w)$ and $\hat{s}_a(\nu,w;X,Y)$ are statistically independent and stationary processes if the continuous random field L(x,y) is a real, Gaussian process. Thus the aliasing component $r_a(x,y)$ can be treated as an additive noise. The Wiener spectrum of the reconstruction can be expressed as : $\hat{\phi}_r(\nu,w) = \hat{\phi}_s(\nu,w) + \hat{\phi}_a(\nu,w)$, which is the sum of signal components that are within the spatial frequency pass-band of the sampling and reconstruction processes, and the signal components introduced by aliasing, $\hat{\phi}_a(\nu,w)$. These latter components are those that fall within

the pass-band of the reconstruction process and can be expressed as :

$$\hat{\phi}_a(\nu, w) = \left[\sum_{m=-\infty,n=-\infty}^{\infty}\sum_{(m,n\neq 0)}^{\infty}\hat{\phi}\left(\nu-\frac{m}{X}, w-\frac{n}{Y}\right)\cdot\left\{\hat{\tau}_s\left(\nu-\frac{m}{X}, w-\frac{n}{Y}\right)\right\}^2\right]\left\{\hat{\tau}_R(\nu, w)\right\}^2$$

where $\hat{\tau}_s$ and $\hat{\tau}_R$ are the spatial frequency responses of the sampling and reconstruction processes respectively. Thus the blur and aliasing errors introduced when a random field of the type described above is scanned can be calculated. The errors computed by Huck et al.(2.7) for the sampling range $0.5 \leqslant s \leqslant 1.0$ were the evaluation of the following integrals :–

for blur : $$\sigma_s^2 = \int_{-\infty}^{\infty}\int_{-\infty}^{\infty}\hat{\phi}_s(\nu, w)\,d\nu.dw \quad , \text{ and}$$

for aliasing : $$\sigma_a^2 = \int_{-\infty}^{\infty}\int_{-\infty}^{\infty}\hat{\phi}_a(\nu, w)\,d\nu.dw .$$

The variance of the input signal, the random field, is given by :

$$\sigma_L^2 = \int_{-\infty}^{\infty}\int_{-\infty}^{\infty}\hat{\phi}(\nu, w)\,d\nu.dw .$$

Plots of these blur and aliasing errors, taken from Huck et al.(2.7) for a random field with $(\mu_7\gamma) = \left(1/3\right)$ scanned with a circular aperture and two types of transmittance profile (one uniform and the other Gaussian), are given below by Fig.2-3 .

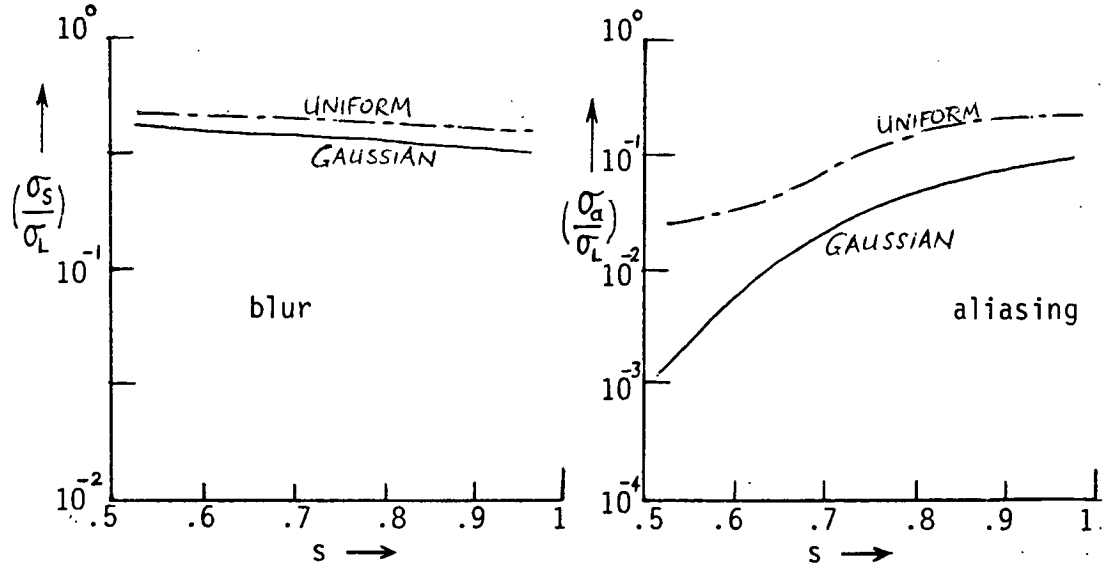

Figure 2-3 : Blur and Aliasing Errors Due to Scanning plotted versus Sampling Interval, s.

It can be seen from Fig.2-3 above that there is a distinct gain in image quality to be had by allowing overlap to occur in scanning systems, even up to the level of s = 0.5, regardless of the transmittance profile of the scanning aperture. There is further improvement in grading the transmittance profile in a form close to Gaussian; this should be possible to do photographically with regular microphotometer apertures, since their minimum diameters are usually of the order of 500 μm., much greater than typical emulsion grain sizes.

The signal-to-noise ratio (SNR) of the combined MPV2 microphotometer and instrument-computer ADC was measured at various levels of illumination, using the normal settings of PMT-voltage and sampling-aperture diameter that are employed in scanning with the 10μm. stepping stage : V_{pmt} = 600 Volts, D_{sa} = 12μm. As has been mentioned above, the SNR values are quite high; the SNR is also best when the illumination is high. See Table 2.1 below :

Illumination Current	Photometer Panel Rdg.	ADC Average (100 Readings)	Standard Deviation	Signal-to-Noise Ratio (Ave./ 2σ)
5.42	1400	191.5	0.086	1110
5.29	1200	164.1	0.056	1470
5.13	1000	137.4	0.046	1490
4.96	800	110.1	0.039	1410
4.75	600	82.9	0.037	1120
4.47	400	55.7	0.028	995
4.06	200	28.4	0.016	888
3.71	100	14.7	0.014	525
3.44	50	7.76	0.012	323

Table 2.1 : Microphotometer/ADC Signal-to-Noise Ratio vs. Illumination.

When scanning photometry is being done there are other sources of image noise, arising primarily from mechanical imperfections in the stage movement. Drift is minimised by allowing the instrument a half-hour to stabilise thermally after turning on.

Chapter 3: Digitisation of Static Television Images.

The standard television monochrome signal in Australia is composed of 625 scanned lines of image, presented at a rate of 25 frames per second. Each of the 25 frames is presented in two interlaced fields of 312 lines, each field-sequence of $\frac{1}{50}$ th second duration. Each line is of 64 micro-seconds duration and is partly composed of a line-synchronising pulse of approximately 5 micro-seconds duration. (3.1). Vertical synchronising pulses occur at 50 Hz and are of approximately 500 μs duration. The start of an interlaced field occurs at a half-line interval after the end of the preceding vertical synchronising pulse. During high-frequency transmission of television signals a train of line-synchronising pulses and equalising pulses (at twice line frequency) are inserted in the period of each vertical synchronising pulse. The presence of picture-intensity information gives the television signal significant spectral components over the range zero to several MHz.

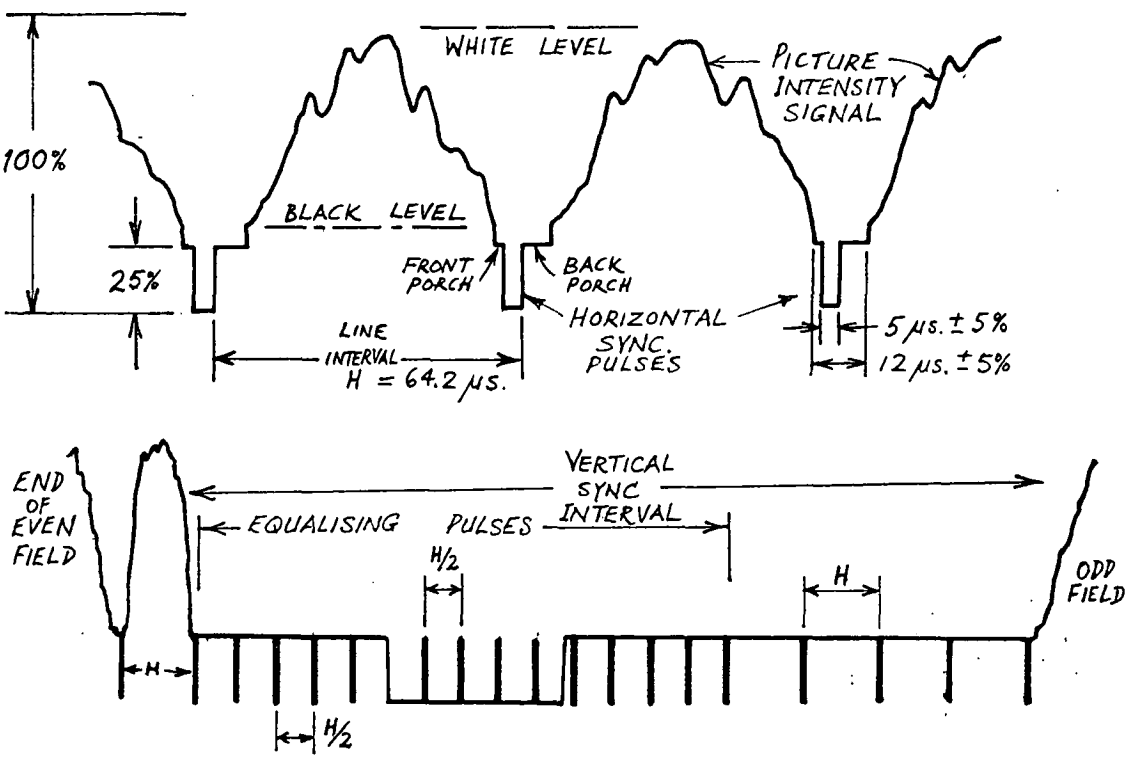

Fig. 3-1 : The Television Signal

Typically the amplitude of the video signal is 1 Volt peak-to-peak, with the top three quarters of the wave-form reserved for the picture-intensity signal, and the bottom quarter reserved for synchronising pulses. Thus a signal of $\sim$ 0.3 Volts would represent zero picture-intensity (black) and a signal of $\sim$ 1 Volts would represent the maximum picture-intensity (white). Clearly there should be a precise control of these maximum and minimum levels if the television camera is desired to be used as a measuring (photometric) camera.

The process of digitising a standard television signal so that it can then be stored in the memory of a computer can be shown to impose rather daunting requirements upon the designer of the electronic hardware. If the image of one monochrome frame of television is assumed to represent 256,000 (512 x 512) bytes of information, then the digitising hardware must transfer this data to a computer memory at an average rate of (256,000 x 25) nearly 8 Megabytes per second to maintain a complete record of a dynamic televised scene. For the purposes of obtaining repeatable digital images of microscope tissue-sections, there are fortunately several simplifying factors.

For tissue sections the televised field of view is generally a static image; thus the signal digitisation can be performed over an interval of many successive frames, at a speed more appropriate to the cycle-time of common microcomputers ($\sim$ 1μs). The diagram below, Fig. 3-2, shows three timing options that could be chosen if interlacing is ignored: Sampling time-sequence = $1,2,3.....n^2-1, n^2$. The two important timing parameters to consider in these schemes are the total digitisation-time, T_d, and the minimum time between sampling instants, t_s. For a (128 x 128)-sample digitisation, T_d and t_s would have minimum values of approximately 0.7 seconds and 10 microseconds respectively, if option 3-2c is chosen.

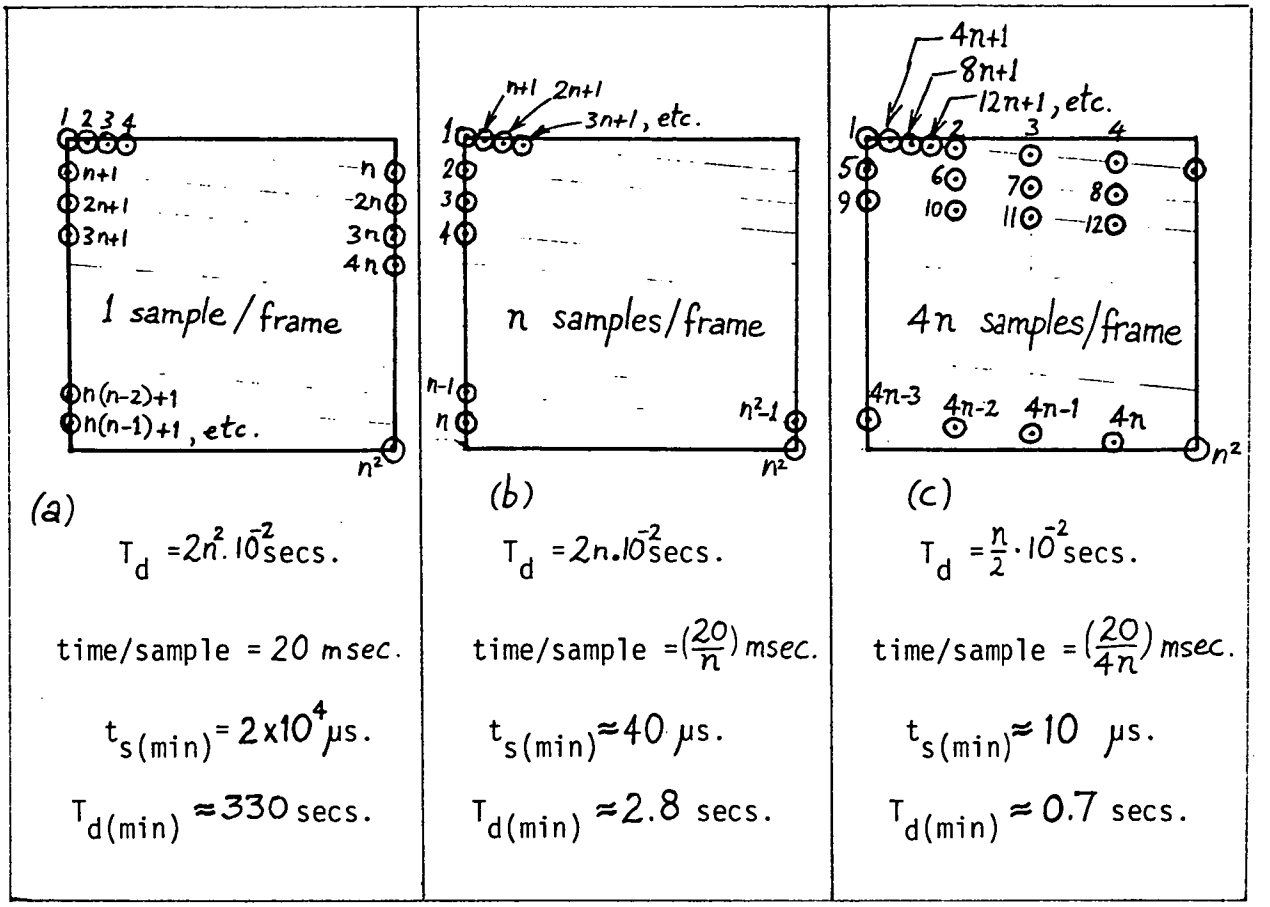

Fig. 3-2: Three (n x n) pixel digitisation sequence options for a static television image.

In keeping with international image-processing standards which favour pixellation at integral exponents of two (3.2), the pixel-value n shown in Fig. 3-2 above could be chosen as 2^7, 2^8 or 2^9 for a standard 625-line image. The sequence option chosen in this study is 3-26, with pixel-values of 128 and 256, a choice dictated by the existing instrument computer, an Acorn Model BBC-B fitted with 20K bytes of additional RAM.

The television camera attached to the QLM is a DAGE type MTI-65 with 1" Vidicon and RS-330 standard signal output. Its specified resolution is 800 lines (at centre); the camera SNR is unspecified, but a typical figure to be expected would be 100:1 (40 dB). Measurements of the SNR gave results between 35 and 40 dB under conditions of illumination chosen for comfortable viewing at the microscope; thus a six-bit digitisation (64-levels) of the video signal is regarded as a suitable degree of precision in amplitude-resolution.

As mentioned above, there is a need for precise control of the gain and thresholds of the television camera if it is to be used as a measuring camera. The following feedback systems in the camera circuit are thus modified: (refer to the camera block diagram, Fig. 3-3).

(a) Automatic target-voltage system: this is disabled by clamping the feedback transistor Q17 in a cut-off condition, allowing manual control of the target-voltage by VR3. The target voltage is fixed at +30 Volts.

(b) Automatic gain-control system: this is disabled by clamping the feedback transistor Q7 in a cut-off condition, thus making gain manually controllable by the setting of VR2. The negative feedback applied to Q12 is reduced by bypassing its emitter series-resistor with a capacitor, thus maximising the gain in the variable-gain stage represented by Q11, Q12 and C15. The automatic bandwidth control is left unaltered.

(c) Automatic black-level system: This system compensates for signal-level drift and dark-current drift due to temperature, tube age and target-voltage changes that occur when the auto-target voltage system is in operation. Since the target voltage is fixed and since the camera could be kept at a constant temperature (in its laboratory environment), it is decided to set the black-level manually and to monitor any variations due to tube age at intervals of no longer than one month. Accordingly the wiper of VR6 is disconnected from the output of QM1 and jumpered to the line-clamp FET, Q13.

As well as ensuring that the image-sensing device has well-controlled and stable operating parameters, it is essential to provide an accurately calibrated source of illumination. Thus a similar calibration to the method required for conventional microphotometry (3.3) is employed. In addition the illumination is filtered with a KODAK Wratten band-pass filter with a 530 nm. central wavelength. This removed spectral variations that will occur

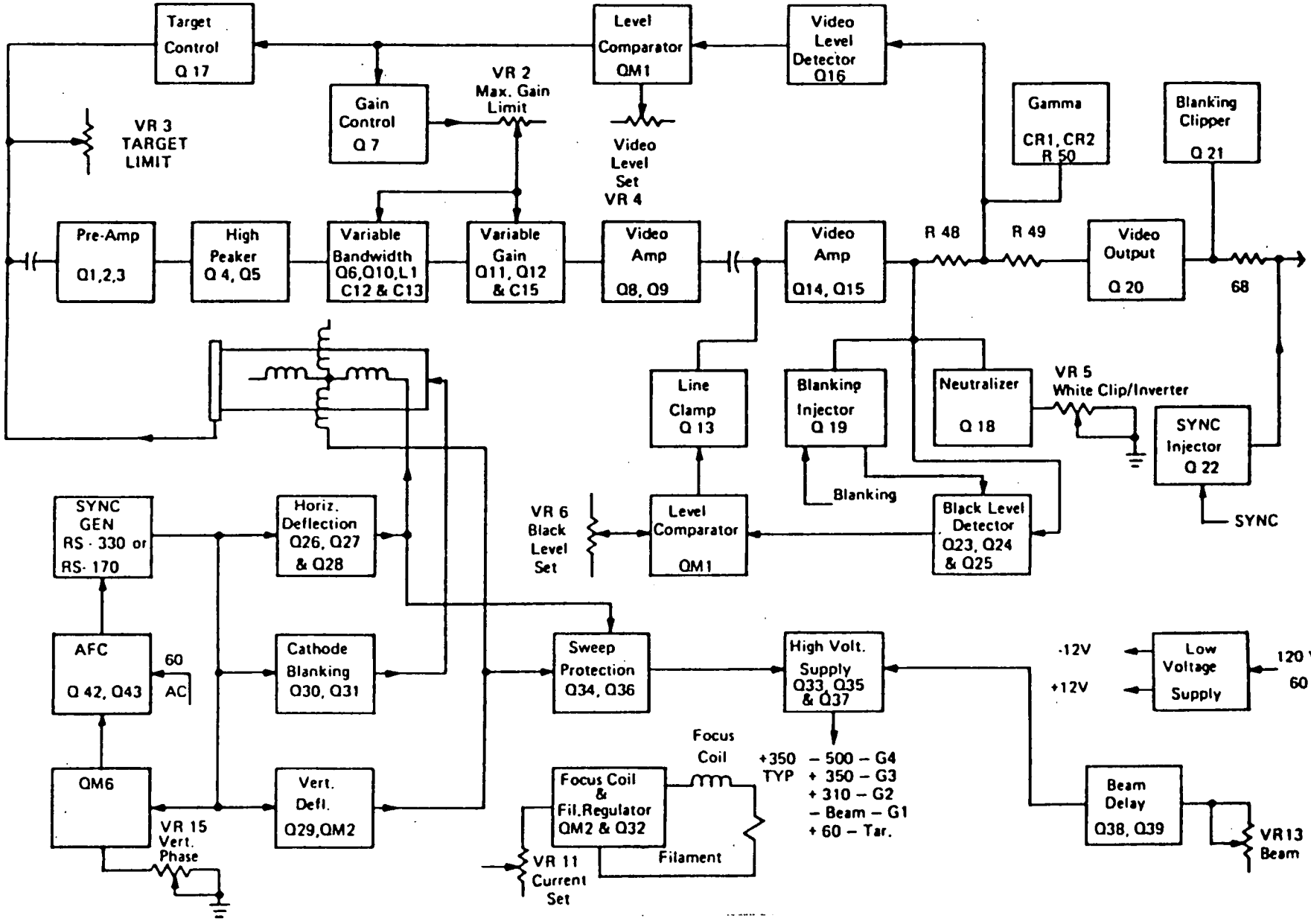

FIG. 3-3 MTI-65 CAMERA Block Diagram

when the illumination filament-current is changed (normally after changing the objective lens power), provided best contrast for the most commonly-used tissue stain (Haematoxylin & Eosin) and provided illumination at a wavelength which is close to the points of maximum sensitivity of both the human eye and the vidicon.

The instrument computer available for the task of signal digitisation and storage, an ACORN BBC-B, possesses a 10-bit ADC with an 8-bit conversion time of 4 milliseconds. Thus an interface is constructed with a much faster ADC (8 μs. conversion) and parallel data-transfer to the computer; its block diagram is shown in Fig. 3-4. A clamp is used to present synchronizing pulses to the comparator at a predictable level and an I.C. video amplifier (National Semiconductors type LM733) is used to provide a signal gain of 2.0 to 5.0, to match the input signal to the input range of the ADC. The ADC chosen is a Ferranti type ZN448 with an on-chip 2.5 Volt bandgap reference.

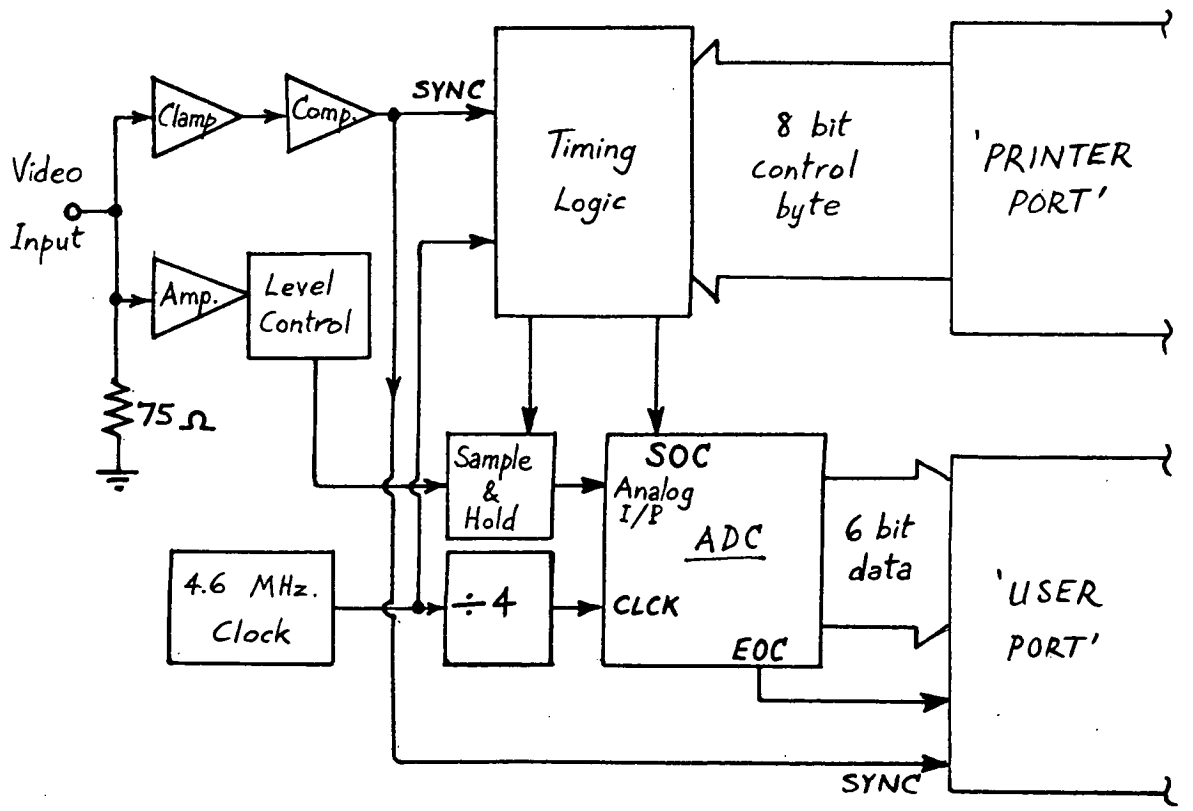

Fig. 3-4: Acorn BBC-B/Video-Signal Digitisation Interface Block Diagram.

Two computer programs have been written in 6502 machine code to breathe life into the hardware described above. They are:

(a) program 'FRAG', to control interface timing while monitoring the TV signal samples. This program operates with all computer interrupts disabled, since it is a time-critical task, and transfers signal samples to magnetic disk in four 16K-byte blocks in the case of 64K-pixel images to circumvent the problem posed by the computer's data-storage RAM which is limited to 16K bytes.

(b) program 'U' to display the image data rapidly (~ 1 sec.) as an eight-colour digital image. An alternative data-display program, written in BASIC, has shown itself to be unconscionably slow (~ 45 seconds), since such a display is usually required only as a quick visual check on system integrity.

Annotated listings of these two programs are attached. (Appendix 1).

Chapter 4 : Quantitation Using the Laplacian Operator

Two of the most frequently encountered problems in the analysis of microphotometric scans are those of simple counting and segmentation. Due to the loss of information inherent in the sampling and reconstruction processes (because of aliasing and the loss of higher spatial-frequency components), the need exists for a quantitative guide to thresholding: it is only when statistically 'good' thresholds have been chosen that accurate segmentation and counting can be done.

The most simple and direct approach to threshold selection is based upon locating minima in the histogram of the scan data. If a substantial amount of sampling-caused blurring of the scan data is present, this approach is inapplicable; a sharpening of the scan histogram can be carried out however using properties of small regions of the scan data based upon mathematical operators such as the Laplacian, particularly if attention is restricted to a particular class of images, such as microphotometric scans.

The Laplacian operator in its original expression is derived from the vector differential operator ∇ (del), by forming its scalar product with itself, $\nabla.\nabla$.

Since $\nabla f(x,y,z)$ is the vector gradient of a function $f\ (x,y,z)$,

$$\nabla f = \underset{\sim}{i}\frac{\partial f}{\partial x} + \underset{\sim}{j}\frac{\partial f}{\partial y} + \underset{\sim}{k}\frac{\partial f}{\partial z}\ ,$$

and $\nabla.\nabla f(x,y,z)$ is the divergence of the gradient, the Laplacian:

$$\nabla.\nabla\ f(x,y,z) = \nabla^2 f(x,y,z) = \frac{\partial^2 f}{\partial x^2} + \frac{\partial^2 f}{\partial y^2} + \frac{\partial^2 f}{\partial z^2}$$

The equation $\nabla^2 f + k^2 f = 0$ has several well-known forms that are invaluable in field theory (4.1), viz. for

(cont'd)

$k^2 = 0$ - Laplace's equation,

k^2 = +ve constant - Helmholtz' equation,

k^2 = -ve constant - Diffusion equation, and

k^2 = constant x kinetic energy - Schrödinger wave equation.

The function f in the case of microphotometric scan data is a scalar function of two discrete variables, the points at which the photometric data is sampled; it is useful to consider the physical meaning that $\nabla^2 f$ assumes in such a case. The second partial derivative of a function of a continuous variable is often referred to as its curvature in that particular variable or dimension. For data sampled in two dimensions the Laplacian value at a point (i,j) is expressed in current literature as the absolute value of the difference between the value at that point, p(i,j), and the average of the adjacent eight neighbouring points, n_8,

where $$n_8 = \frac{1}{8}\left(\left\{\sum_{i-1}^{i+1}\ \sum_{j-1}^{j+1} Pij\right\} - Pij\right), \quad (4,2).$$ Such an expression

will give large values in highly discontinuous regions, where edges, holes and other dislocations exist in tissue sections for example, unless the central point is within discontinuous regions that may be best likened to 'saddle' surfaces (of opposite curvature in two orthogonal directions) and regions of very high, uniform slope. To determine the frequency of occurrence of such central points a survey was made of twenty microphotometric scans of several types of natural tissue sections; the results are shown here in Table 4.1. The analysis program is attached in Appendix 2.

The program, 'LAP', calculates the number of anomalous "saddle'-points by testing the products of pairs of differences between opposing neighbourhood edge-points, and the central value of that (3X3) neighbourhood. If either of the products is less than -99 then it is classified as anomalous. All scan values dealt with are integers in the range zero to one-hundred.

Points are classified as 'anomalous & high-slope' by the program if

Table 4.1 : Statistics of Anomalous Laplacian Points in Twenty Microphotometric Scans.

TISSUE TYPE	STAIN	POINTS WITH LAPLACIAN >10 (% of total)	SADDLE POINTS (% of total)	POINTS OF HIGH SLOPE (% of total)
Human Prostate	H & E *			
# 1		4.44	3.22	3.76
# 2		2.46	2.32	1.88
# 3		2.76	1.85	1.56
# 4		20.1	11.3	10.5
# 5		0.59	0.49	0.098
Human Skin	Warthin-Starry			
# 1		10.7	8.20	2.80
# 2		1.66	0.80	0.27
# 3		19.6	16.2	13.0
# 4		1.85	1.78	0.85
# 5		19.5	11.4	5.78
Human Breast	H & E *			
# 1		1.98	0.83	0.73
# 2		1.54	1.12	0.12
# 3		0.37	0.22	0.024
# 4		0.39	0.20	0.049
# 5		0.61	0.54	0
Pacific Oyster, C.Gigas	Timms			
# 1		12.5	11.3	9.68
# 2		12.8	8.95	5.63
# 3		13.4	10.1	8.10
# 4		5.27	4.34	2.56
# 5		8.63	7.39	2.95

* "H & E" indicates Haematoxylin and Eosin

they have been first rejected as Laplacian or saddle-points, and if one-eighth of the sum of the absolute values of all differences (between the central point and its eight neighbours) exceeds the Laplacian difference-threshold, the 'similarity-parameter', S% in the program. This classification would typically be given to points possessing two groups of four neighbours that are relatively very high and very low by roughly equal amounts.

Table 4.1 shows that the discrete form of the Laplacian operator is generally valid as a means of locating discontinuities in microphotometric scans; indeed the use of this operator to sharpen histograms of such scans and to locate thresholds for the counting of small, dark points in oyster tissue sections (representing metal-bearing granulocytes) is the subject of a recent publication by the author and colleagues (4.3). Nevertheless there is a disturbing trend in Table 4.1 for anomalous points to be present in numbers similar to the total of Laplacian points, prompting one to look for an operator yielding greater accuracy. Another feature of this table is that there is potentially useful information in the relative numbers of anomalous points, with regard to texture. In the scans of prostate tissue, for example, there is a consistently lower number of discontinuity-points in areas that are free of cancer; scan #5 is an instance of this. Scans #3 and #4 differed only in the depth of staining, so this is another factor that affects the results of counting with program 'LAP'.

An alternative edge-detection operator is the isotopic derivative form known as the gradient. For the continuous function f(x,y) it has a magnitude and direction given by $\left[\left(\partial f/\partial x\right)^2 + \left(\partial f/\partial y\right)^2\right]^{1/2}$ and $\arctan\left[\left(\partial f/\partial x\right)/\left(\partial f/\partial y\right)\right]$, (4.7). In its discrete form the magnitude can be expressed as the average of the absolute values of differences between opposite points of a 3X3 neighbourhood, calculated for two orthogonal scan axes. A comparison of the numbers of points having a gradient magnitude greater than ten with the corresponding numbers of Laplacian points for the same scans is shown in Table 4.2, below.

All twelve scans are over prostate tissue sections and the table shows that points with a high gradient magnitude are far more common than points with a high Laplacian value. In contrast to the Laplacian operator the gradient operator is not strongly affected by tissue-staining, and there is no overlap between the counts for the two sets of four scans taken over the same slide, comparing two areas judged to be different from the clinical pathologist's viewpoint.

Table 4.2: Comparison of Laplacian and Gradient Point Numbers.

Scan title	Pathology (all Prostate)	Laplacian (threshold =10,	Gradient both as % of total)
D.B1	Cancer, light staining.	4.44	23.6
D.B2		2.46	16.9
D.B3		2.76	14.2
D.B4		2.02	12.6
D.B11	Cancer, heavy staining.	21.9	46.1
D.B12		22.8	44.2
D.B13		20.1	42.7
D.B14		16.4	33.2
D.Y1	Benign, medium staining.	2.15	9.29
D.Y2		1.15	5.29
D.Y3		0.59	2.85
D.Y4		1.49	7.95

Other neighbourhood-operators that can be used in histogram-enhancement are the Roberts-Cross (4.2), various forms of the Laplacian taken over wider areas (4.4), and operators that select the maximum of differences of average values in pairs of horizontally and vertically adjacent 2x2 neighbourhoods. Alternative approaches to segmentation employ iterative methods to modify the histogram (4.5) and probabilistic relaxation of individual point values (4.6). An operator that shows more promise as a means of enhancing textural detail is the Sobel operator (4.8), which will be considered at length in the next chapter.

CHAPTER 5: Texture Analysis of Tissue sections

Several definitions of image texture have been proposed, but as yet there is none that has been accepted universally. There have been several good reviews of texture (5.1, 5.2, 5.3); all of them agree that 'natural' texture is a stochastic or deterministic surface-property repeated over locales and that local properties can best be assessed by reference to the concept of a textural primitive. There is good evidence to show that image statistics beyond the second-order level are relatively indistinguishable by the human visual system (5.4), thus raising the hope that visual automata can achieve a level of performance quite beyond the ability of human observers in the assessment of natural textures.

In the absence of well-defined shape or structural primitives a statistical approach to texture analysis is likely to be more effective; this is the case with the great majority of the biological tissue sections that the author has encountered. Biological organisms evidently have ordered structures, but such is their variability at all levels of size that a structural approach to their textural properties was judged to be unlikely to meet with success. Thus the problem becomes one of deciding which set of statistical features is likely to be most effective in providing a satisfactory analysis of the natural textures in tissue sections. Fortunately there is a good guide in the results of tests by Pratt, Faugeras and Gagalowicz (5.7) and by Faugeras and Pratt (5.8), where texture feature-extraction methods were developed from a stochastic texture model. This model views each texture-region as a sample of a two-dimensional stochastic process which can be described by its statistical parameters, particularly its first four moments - the average, variance, skewness and kurtosis. An eight-dimensional texture-feature vector is obtained from the autocorrelation function of the texture field, using its first four moments, and from the histogram of the texture field after a decorrelation

process. Classification of four natural textures (sand, grass, wool and raffia) by this method was shown to be quite good (5.8); a simplification of the method arises from noting that the histogram moments of decorrelated fields are good discriminant features by themselves.

The operator chosen for decorrelation of the tissue-section scans in this study is the Sobel operator, which can be understood by reference to Figure 5-1 below : The Sobel value at each point 't' is given by

$$S_t = \left[(p+2q+r-v-2w-x)^2 + (r+2u+x-p-2s-v)^2 \right]^{1/2}$$

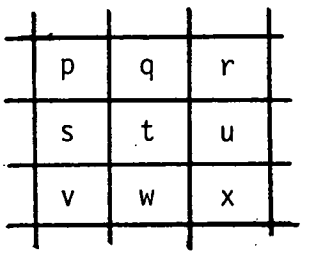

Figure 5-1 : The (3X3) mask-size Sobel Operator

A program, 'SOBEL', was written to perform this decorrelation of the microphotometer scans; see Appendix 2. The Sobel operator was chosen because it performs well in comparison with other edge-detection and thresholding operators such as the Kirsch, Roberts, Laplace and Prewitt operators (5.11). An extension of the mask-size (beyond the 3X3 level) was thought unnecessary in view of the relatively high signal-to-noise ratio ($>$100:1) of the microphotometric scans; this also confers greater computational simplicity and speed.

Texture analysis is a pattern recognition problem; the feature-vector $\underset{\sim}{v}$ must be chosen so that its constituent set of measurements v_i condenses the essential properties of the texture-field into a 'feature-space' (5.3), whereby recognition of the texture is facilitated. A figure-of-merit for the choice of measurements in this study, indicating the separation of classes in feature-space, is therefore given for all pairs of measurements by a statistical analysis of covariances.

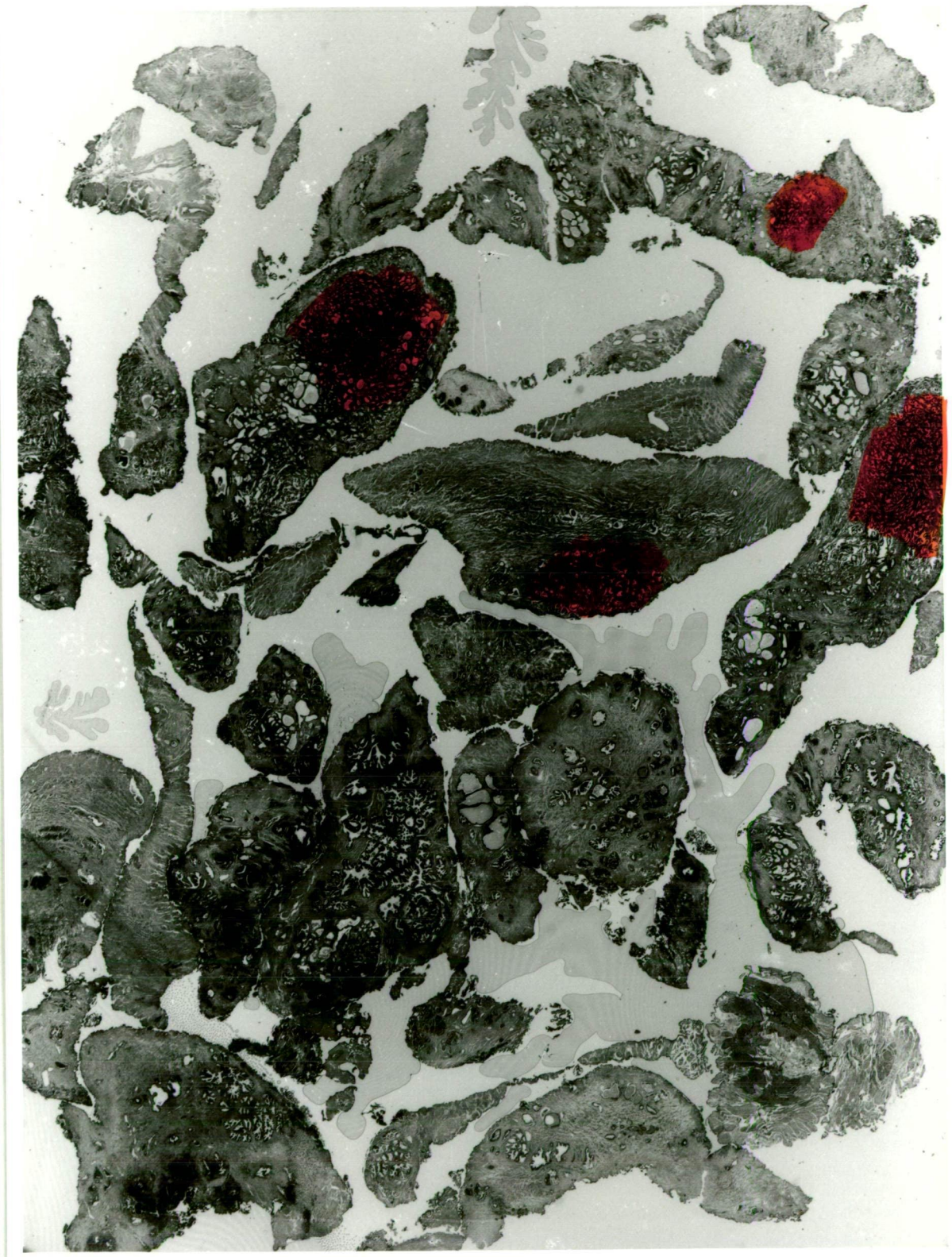

Figure 5-2 : Photograph of the Prostate Tissue Section, Slide S1, that was scanned microphotometrically. Several areas of the tissue (shaded) are carcinomatous.
MAG'N. ×6.5

The test objects for texture analysis were two Haematoxylin/Eosin-stained, 5 μm.-thick, stepped sections of human prostate tissue, slides S1 and S2. Twenty-eight areas of 1.6 mm^2 were scanned microphotometrically in 10 μm. steps over square grids of 16,384 points each. Eight scans were carried out initially on S1 over areas judged to be texturally different by a non-specialist. This naïve selection of areas was then re-scanned after the tissue section had been re-stained to test for variation of the texture indicators. Slide S2 was prepared six months after S1, during which time the tissue block was subject to the minor effects of storage in paraffin at room temperature. Approximately 30 μm. of the block was removed in cleaning the face to be sectioned for the preparation of S2; the appearance of S2 after Haematoxylin / Eosin staining was very similar to, but not identical with, Slide S1. Twelve 1.6 mm^2 areas were scanned microphotometrically on S2, following a dispersed selection similar to that on S1. As is the usual practice with (H & E) stained tissue, green light (KODAK Wratten Filter No. 58) is used to illuminate the tissue for maximum contrast.

At the start of each series of scans the instrument is allowed a half-hour to stabilise thermally and the photometer ADC is calibrated. The measuring stop was adjusted to a width of 12 μm., referred to the image (tissue-section) plane, and the luminous-field stop was adjusted to a width of 30 μm. in the same plane to minimise diffraction disturbances from its edge. A 100% transmission reading was obtained close to each scan area, through an area of slide clear of tissue within a 60 μm. radius. At the end of each scan the data was rejected if more than 1% of the 16,384 transmission readings were in excess of 100%. In this way a reasonable degree of standardisation was achieved.

The results of each microphotometric scan were analysed statistically to derive the mean, variance, skewness, kurtosis and span values. The span was taken to be the separation between the 5th and 95th percentiles.

Each scan was processed with the Sobel operator, as outlined above, and the same statistics were obtained from the processed scans. The Sobel-processed scans showed enhancement of discontinuities in the original scans, as can be seen by the digital image pairs of Figure 5-3.

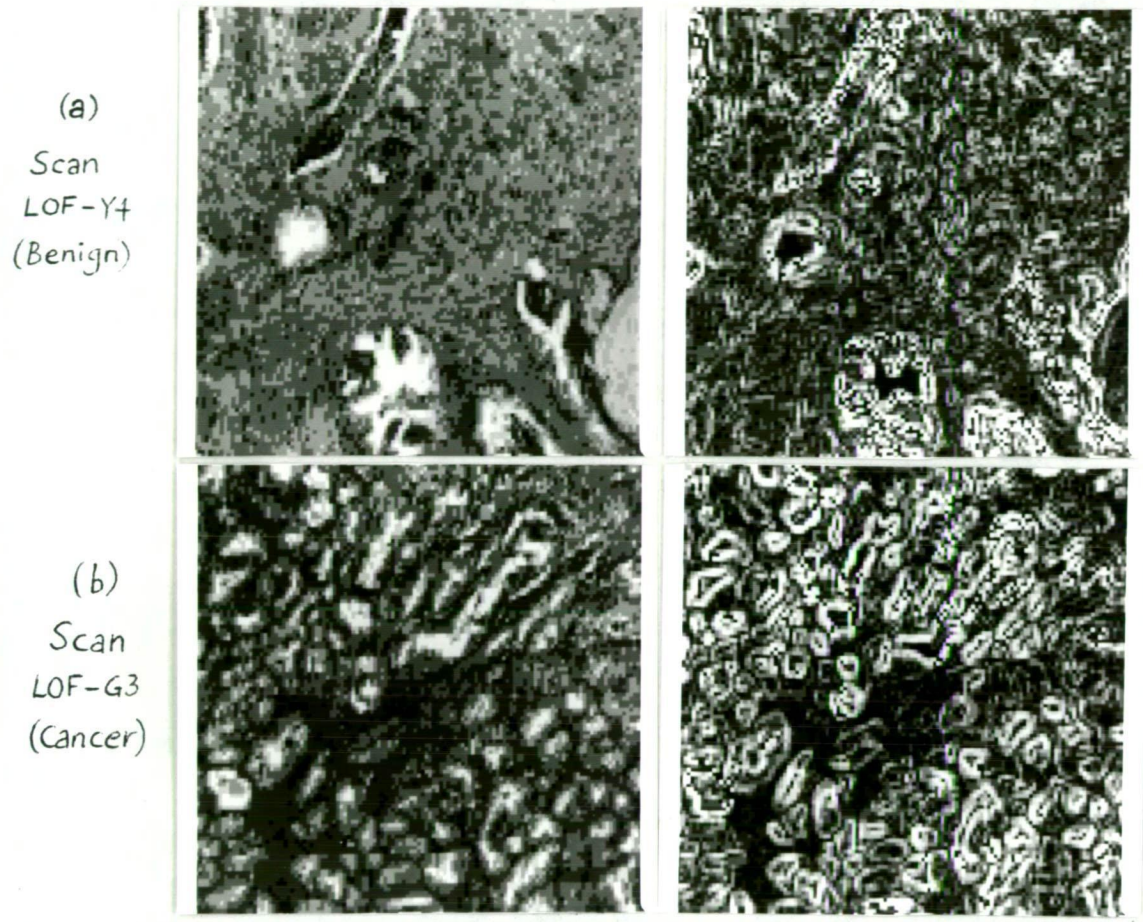

Figure 5-3 : Two digital-image pairs at the same thresholds, showing the edge-enhancement due to processing with a Sobel operator. Unprocessed scans are at left, processed at right.

Tables 5.1 and 5.2 show the statistics for the unprocessed and processed scan data, respectively. All of these scan areas were examined by medical specialists so that a 'cancer' or 'benign' classification could be given. The letter C or B indicates this expert opinion; a small 'm' subscript indicates a majority opinion.

Twenty scans were selected, whose assessments by the specialists were unanimous, with ten being in each of the two classifications. These have been

Table 5.1 : Statistics of Twenty-Eight Microphotometric Scans of Prostate Tissue

SCAN Area	Pathology	Mean	Variance	Skewness	Kurtosis	Span
LOF-B1 * 1.	C	81	61	0.93	3.22	26
LOF-B2 * 2.	C	83	54	0.73	3.18	26
LOF-G1 * 3.	C	78	70	0.88	2.90	27
LOF-G2 * 4.	C	75	53	1.27	4.20	24
LOF-R1 *11.	B	76	80	1.34	4.08	32
LOF-R2	C_m	80	115	0.64	2.29	31
LOF-Y1 *12.	B	84	39	0.13	3.98	21
LOF-Y2 *13.	B	81	45	0.85	4.43	26
LO-B1 * 5.	C	65	240	1.11	2.91	49
LO-B2 * 6.	C	64	207	1.12	3.08	46
LO-G1 * 7.	C	62	259	0.96	2.80	52
LO-G2 * 8.	C	58	181	1.71	4.98	46
LO-R1 *14.	B	61	189	1.72	4.89	49
LO-R2	C_m	67	312	0.80	2.05	49
LO-Y1 *15.	B	69	87	1.01	4.40	32
LO-Y2 *16.	B	67	96	1.48	5.23	39
LOF-B3 * 9.	C	78	72	0.65	3.20	30
LOF-B4 *10.	C	73	72	1.05	3.72	28
LOF-B5 *17.	B	83	27	0.46	5.36	17
LOF-B6 *18.	B	83	21	0.42	5.56	15
LOF-G3	B_m	80	55	0.69	3.73	26
LOF-G4	B_m	76	47	0.93	4.64	24
LOF-V1	C_m	78	77	0.65	2.74	30
LOF-V2	C_m	80	102	0.50	2.13	30
LOF-W1	B_m	75	67	1.40	4.73	30
LOF-W2	B_m	76	44	1.30	5.55	21
LOF-Y3 *19.	B	75	52	0.83	4.67	24
LOF-Y4 *20.	B	74	66	0.85	4.04	29

C = Cancer B = Benign

C_m = Cancer, admixed with other pathological classes

B_m = Benign, admixed with other pathological classes

Table 5.2: Statistics of Twenty-Eight Sobel-processed Scans

SCAN Area	Pathology	Mean	Variance	Skewness	Kurtosis	Span
S.LB1 * 1.	C	34	598	0.93	3.17	78
S.LB2 * 2.	C	31	473	0.95	3.47	69
S.LG1 * 3.	C	35	733	0.87	2.81	85
S.LG2 * 4.	C	30	566	1.03	3.35	75
S.LR1 *11.	B	27	810	1.57	4.74	92
S.LR2	C_m	38	1000	0.91	2.80	100
S.LY1 *12.	B	24	358	2.03	8.56	57
S.LY2 *13.	B	25	449	1.99	7.44	70
S.B1 * 5.	C	44	1145	0.78	2.54	109
S.B2 * 6.	C	52	1087	0.87	2.75	107
S.G1 * 7.	C	48	1077	0.60	2.38	106
S.G2 * 8.	C	38	1029	1.05	3.14	103
S.R1 *14.	B	28	831	1.60	4.92	93
S.R2	C_m	39	1139	0.94	2.86	108
S.Y1 *15.	B	30	508	1.63	6.13	72
S.Y2 *16.	B	28	628	1.93	6.61	85
S.LB3 * 9.	C	36	518	0.88	3.44	74
S.LB4 *10.	C	30	531	1.04	3.71	72
S.LB5 *17.	B	19	205	1.81	8.21	43
S.LB6 *18.	B	19	164	1.32	5.21	40
S.LG3	B_m	30	479	1.31	4.57	69
S.LG4	B_m	27	416	1.50	5.29	66
S.LV1	C_m	34	613	1.00	3.53	79
S.LV2	C_m	32	774	1.18	3.78	90
S.LW1	B_m	27	509	1.53	5.30	72
S.LW2	B_m	25	386	1.65	6.10	62
S.LY3 *19.	B	22	346	2.34	10.11	55
S.LY4 *20.	B	28	490	1.80	6.72	72

C = Cancer B = Benign

C_m = Cancer, admixed with other pathological classes

B_m = Benign, admixed with other pathological classes

marked in tables 5.1 and 5.2 with an asterisk and a numbered sequence. The complete results of the above tables were used to prepare several feature-space diagrams, Figs 5-4 to 5-7, which show four scatter-plots by which the statistics were examined to proved a basis for classification. A two-fold partition of these scatter-plots can be made into the classifications 'Cancer' and 'Benign' with varying degrees of success. A program, 'BAT', was written to provide a quantitative guide to the separation of these two classes (see Appendix 2); table 5.3 shows these separation statistics, known variously as Bhattacharyya or Mahalanobis distances in the literature (5.8, 5.9, 5.10), for all possible dissimilar pairs of statistics that are listed below:

UNPROCESSED DATA	SOBEL-PROCESSED DATA
1. Mean transmission	6. Mean
2. Transmission Variance	7. Variance
3. Skewness	8. Skewness
4. Kurtosis	9. Kurtosis
5. Span	10. Span

Table 5.3: Mahalanobis Distances for Pairs of Scan Statistics, D_{rs}

	STATISTIC (s)								
STATISTIC (r)	2	3	4	5	6	7	8	9	10
1	10.3	1.90	44.5	5.85	82.2	23.1	160	93.9	19.2
2		6.97	41.7	9.15	107	17.0	162	91.2	13.1
3			48.6	4.49	55.0	18.0	160	103	18.0
4				40.3	63.6	44.8	186	125	43.0
5					122	27.7	160	94.8	22.4
6						73	170	104	74.7
7							160	90.6	14.0
8								168	160
9									91.8

The method used for the calculation of these distances is based on an

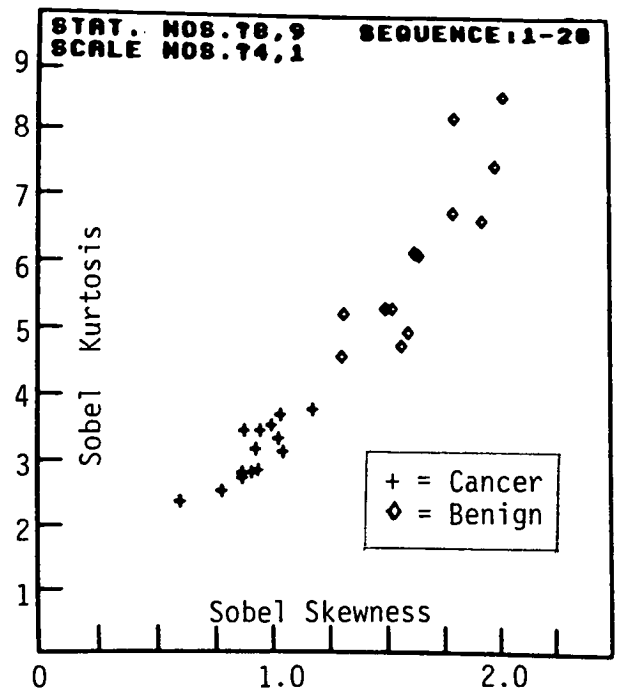

Fig.5-4: Feature-space diagram, Sobel Skewness vs. Sobel Kurtosis. Mahalanobis Distance ≈ 168

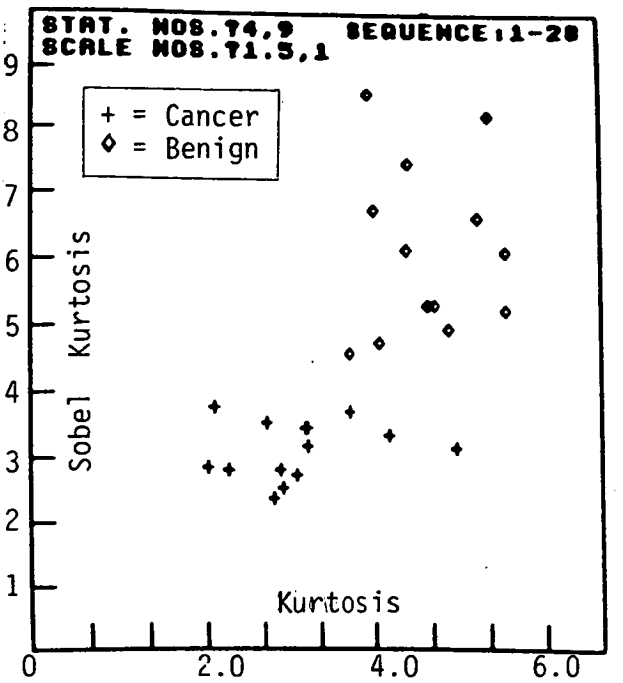

Fig.5-5: Feature-space diagram, (Unprocessed) Kurt. vs. Sobel Kurt. Mahalanobis Distance ≈ 186

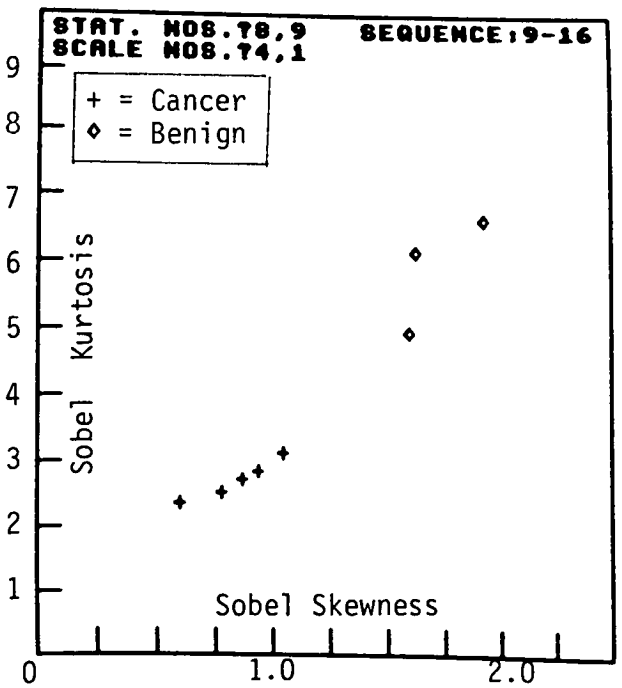

Fig.5-6: Feature-space diagram, Sobel Skewness vs. Sobel Kurtosis. Heavily-stained series, 8 scans.

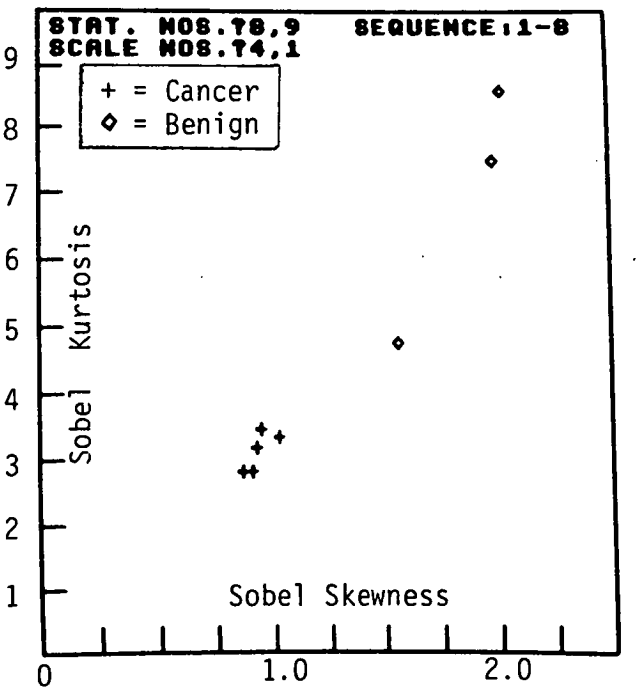

Fig.5-7: Feature-space diagram, Sobel Skewness vs. Sobel Kurtosis. Lightly-stained series, 8 scans.

analysis of covariance and can be understood by reference to Appendix 4 and standard texts on statistics and clustering analysis (5.5, 5.12). The Drs value for the case (r = 4, s = 8) provides support for the inclusion of the histogram moments of unprocessed data in the feature vector; the reason for statistic no. 4, the kurtosis of the unprocessed scan histogram, being such an effective texture-feature is not understood by the author and could well serve as an interesting topic for further research. Another interesting separation value is $D_{8,10}$, whose relatively high level was quite unexpected.

Many other natural textures could possibly be classified rapidly by the above method; future work will broaden the field of application and hopefully shed light on the unanswered questions above. A considerable increase in speed will result from the use of digitised television scans and the conversion of the decorrelation program to machine code. Program SOBEL is currently in BASIC and takes 15 minutes to decorrelate a 16,384 - point scan. For the small number of areas scanned in this study it has been shown that the higher statistical moments of their decorrelated fields can give very effective values for the discrimination of cancerous tissue on a textural basis. In addition it appears that the method has the advantage that it is relatively insensitive to variations in staining intensity.

Chapter 6 : Microspectrophotometry

The properties of a specimen that can be measured with a microphotometer are wavelength-dependent. The useful range of wavelengths of microscope optics is from about 300 to 1100 nm., spanning three regions: the ultra-violet (300 to 400), the visible (400 to 700) and the near infra-red (700 to 1100 nm.). Thus it was decided to couple the MPV2 microphotometer to a monochromator, when an Optica type CF4 was made available in 1982, to make possible the analysis of microscope specimens by microspectrophotometry.

A typical spectrometer consists of an entrance aperture, a collimating element, a dispersing element, a focussing element and an exit aperture. All of these components were available in the Optica CF4, as well as sample compartments placed just after the exit aperture and an obsolete type of photo-detector. The collimating element serves to make all the rays passing through the entrance slit parallel and the dispersing element acts as a filter to separate light rays according to their wavelength.

The expression relating an observed spectral power distribution $I(\lambda)$ to the instrumental profile $F(\lambda)$ and the spectral power distribution of the source of radiation $S(\lambda)$ is one of convolution:

$$I(\lambda) = 2\int_{u=0}^{u=\infty} S(u)\, F(\lambda - u).du$$

Two spectral lines may be regarded as resolved if they can be detected as two lines without the aid of a deconvolution (working backwards to $S(\lambda)$ in the above equation) or knowledge of the instrument profile. The Rayleigh criterion is that two diffraction-limited profiles, with zeros on either side of their principal maxima, are resolved if the zero of one is superimposed on on the principal maximum of the other. Thus the resolution of a spectrometer which can just resolve two maxima at λ_1 and λ_2 is defined as

$$\Delta\lambda = \lambda_2 - \lambda_1$$

and the resolving power as

$$R = \frac{\lambda}{\Delta\lambda}$$

Apart from resolving power, the other basic instrumental factor of a spectrometer to be considered is its flux-gathering power, or étendue. Etendue is conserved in an ideal spectrometer; there will always be one limiting aperture in the instrument which defines one angle explicitly and all the others implicitly. A diagram showing the limits of étendue and resolving power of several common types of spectrometer is shown below by Fig. 6-1, taken from a text by James and Sternberg (6.1).

Several methods of expressing optical absorption are in current use, but all of them are based on the equation $a = k \log_{10}\left(\frac{Io}{I}\right)$, where

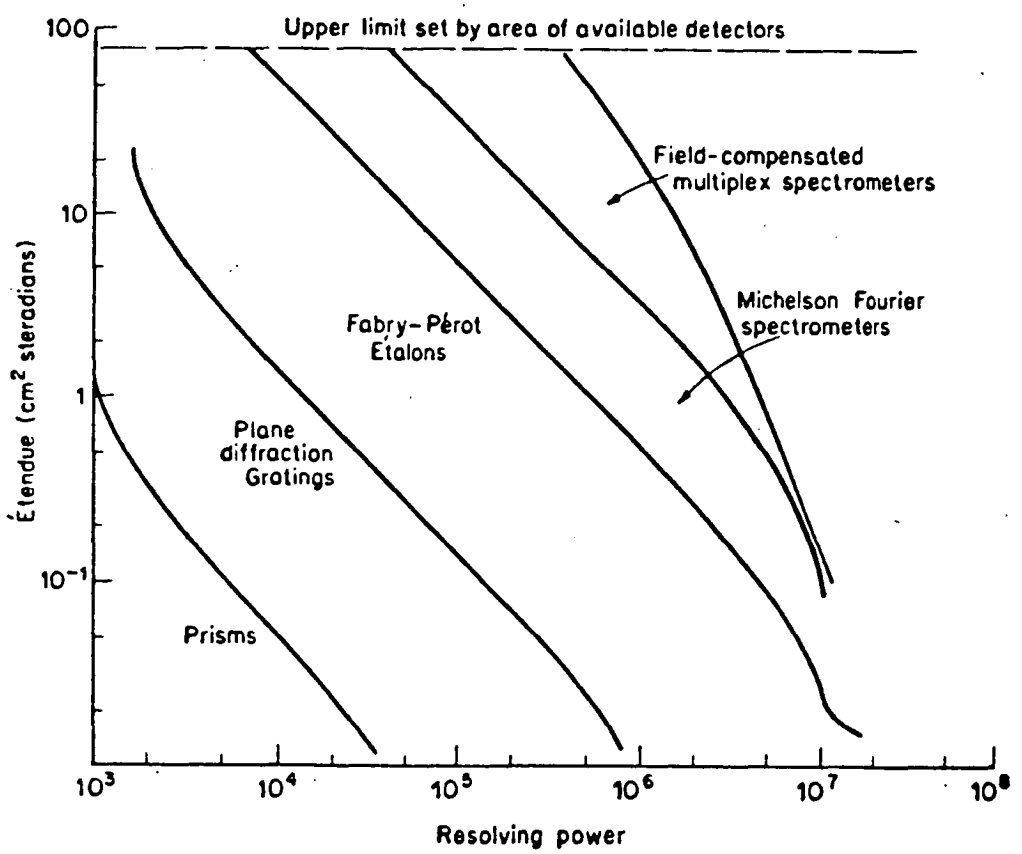

Figure 6-1 : The Performance Limits of Several Types of Optical Spectrometer in Common Use.

k is a constant dependent upon the particular instrument and measurement conditions, Io is the incident light intensity and I is the emergent light intensity. The most common terms are summarised in Table 6.1, below;

't' is the optical path-length in the medium and C is the concentration of the absorbing species in moles/litre.

Term	Symbol	Equation
Transmission	T	$T = \frac{I}{Io}$
Absorption	A	$A = 1 - T$
Optical Density	O.D.	$O.D. = \log_{10}\left(\frac{Io}{I}\right)$
Extinction Co-efficient	α	$\alpha = \left[\log_{10}\left(\frac{Io}{I}\right)\right]/t$
Molar Extinction Co-eff.	ε	$\varepsilon = \left[\log_{10}\left(\frac{Io}{I}\right)\right]/ct$

The OPTICA CF4 is a single-beam, manually-operated spectrophotometer

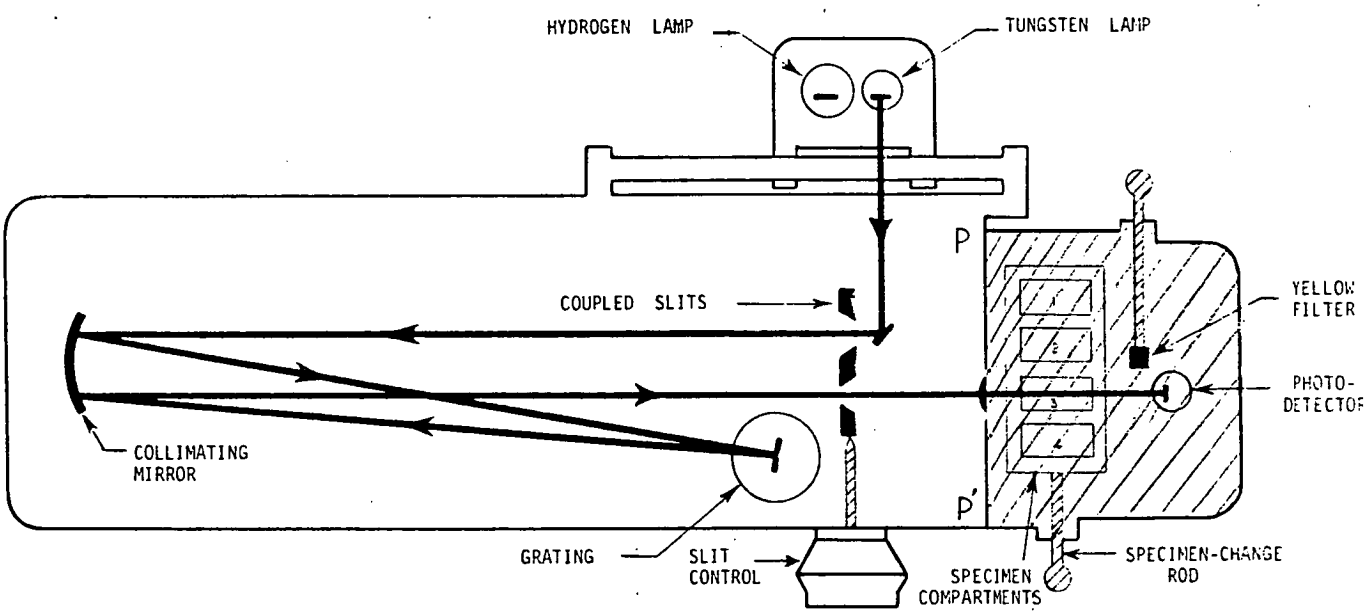

Figure 6-2: The Optica CF4 Spectrophotometer, before the removal of the sample/measurement section.

that has entrance and exit slits with a free height of 0.02m. Its optical layout is shown above, in Fig.6-2. The shaded section containing the specimen compartments, light-detector and yellow filter was removed so that the monochromator could be coupled to the side of the microphotometer at plane P-P'.

A bench with a sliding table was made to support the monochromator so that it could be quickly changed with the usual light-source of the microphotometer, a 100-Watt tungsten lamp. The alignment of the monochromator output to the microscope so that it could form a stationary illuminated field as the wavelength was changed at the specimen stage was difficult, mainly due to the monochromator's mass, ~ 100 kg. Once this was done any further movement was restricted to translation, directly in or out. By using the CF4 monochromator as an alternative illuminator for the MPV2 microphotometer in this way the possibility of stray light entering the system was much reduced.

A plane diffraction grating with 600 lines/mm (15,000 lines/inch) is used in the Optica CF4 and covers the spectral range 185 to 1000 nm. The resolving power of a grating, where N is the number of lines in the grating and m is the order of diffraction, is given by (6.3):

$$R = Nm$$

The plane grating can be regarded as a row of equidistant slits transmitting a plane wave of light parallel to the plane containing the slits. Each slit emits a series of Huygenian wavelets which expand in all directions; the wave-fronts are envelopes of these wavelets and will have angles to the plane of the grating in some way proportional to m and to the inverse of the slit separation, S.

The exact relation is given by:

$$\frac{m\lambda}{S} = \sin\theta + \sin\theta'$$

Table 6.2 below shows the angular spreads for the first three spectral orders of diffraction, for the Optica CF4 grating, considering only the range of wavelengths detectable by the MPV2 photo-multiplier, an EMI type 9558B with S-20 photo-cathode.

Table 6.2: Calculated Angular Spread of Several Successive Orders

λ (nm.)	Θ (deg.) m = 1	m = 2	m = 3
400	13.9	28.7	46.1
500	17.5	36.9	64.2
600	21.1	46.1	> 90
700	24.8	57.1	> 90
800	28.7	73.7	> 90

The considerable degree of overlap here indicates why only the first order of diffraction is used in the CF4, as in many spectrometers. An OR2 glass filter is supplied with the CF4 to remove the second spectral order when measurements are being taken at wavelengths greater than 620 nm. Thus the attainable resolving power of the CF4 can now be calculated; the number of lines in the grating is (length, 4 cm; x N) 2.4×10^4, so

Resolving Power = 24,000

Thus it should be possible to resolve details of ~ 0.02 nm. at a wavelength of 400 nm. (extreme blue). The figure given by the manufacturer is in fact 0.05 nm. In view of the age of the monochromator and the maximum resolution likely to be required in usual applications (~1 nm.), these figures for the attainable resolving power were regarded as more than satisfactory. Experience has since shown that it is the total light available from the monochromator's 50 Watt Tungsten lamp that constitutes the limiting factor in most applications: resolving power is often sacrificed for illumination by opening the slits.

The entrance and exit slits of the monochromator are coupled and are controlled manually at a front panel. The wavelength control is linear, over a metre long and calibrated in 0.5 nm. steps for manual control over the range 185 to 1000 nm. Wavelength is now controllable by the instrument computer by

means of a geared stepping motor attachment to the original manual control The instrument computer monitors the wavelength, to a resolution better than 1 nm., by means of the third channel of its four-channel, 10-bit ADC. This ADC reads the output of a 10-turn, 10KΩ potentiometer whose shaft is geared to the main gear-wheel of the wavelength-control shaft, and to which a highly-regulated reference voltage is applied. The equation relating the monochromator wavelength to the value read by the ADC, A_3, has been found by measurement to be:

$$\lambda = \left\{\left(A_3 / 70.74\right) + 158\right\} \text{ nm.}$$

This relationship is an integral part of a series of programs that have been written to perform the collection of spectra from areas of specimens down to the level of a micron square. Program 'SPAA' is attached, in Appendix 3 . The light-intensity signal detected by the MPV2 photometer tube is digitised by channel 1 of the instrument computer's ADC, in the usual way; depending upon the particular measurement a degree of averaging is carried out to improve the signal to noise ratio.

Since the instrument is of the single-beam type, program SPAA collects a reference spectrum from a clear area of the microscope slide before the specimen itself is examined. All light readings from the specimen are expressed as a ratio to the readings obtained at the same wavelengths in the reference spectrum.

The microspectrophotometer described here has been used for a wide variety of mineralogical and biological specimens in the Central Science Laboratory. Determinations of pleochroism have been made, for minerals whose absorption varies with their principal crystal axes, as can be quickly seen by observation in polarized light. Stains used in sections of biological tissues have been examined, particularly the very common Haematoxylin/Eosin combination that has been shown to have a strong minimum of transmission at

535 nm. The results of this work were presented at the 1984 Symposium of the Royal Australian College of Pathologists in Perth (6.4). An absorption spectrum of a sample of Neodymium-containing glass is shown below, Fig.6-3, illustrating the result obtained when an X-Y plotter was used. Spectra are normally printed out via an ITT Model 43 Teletype.

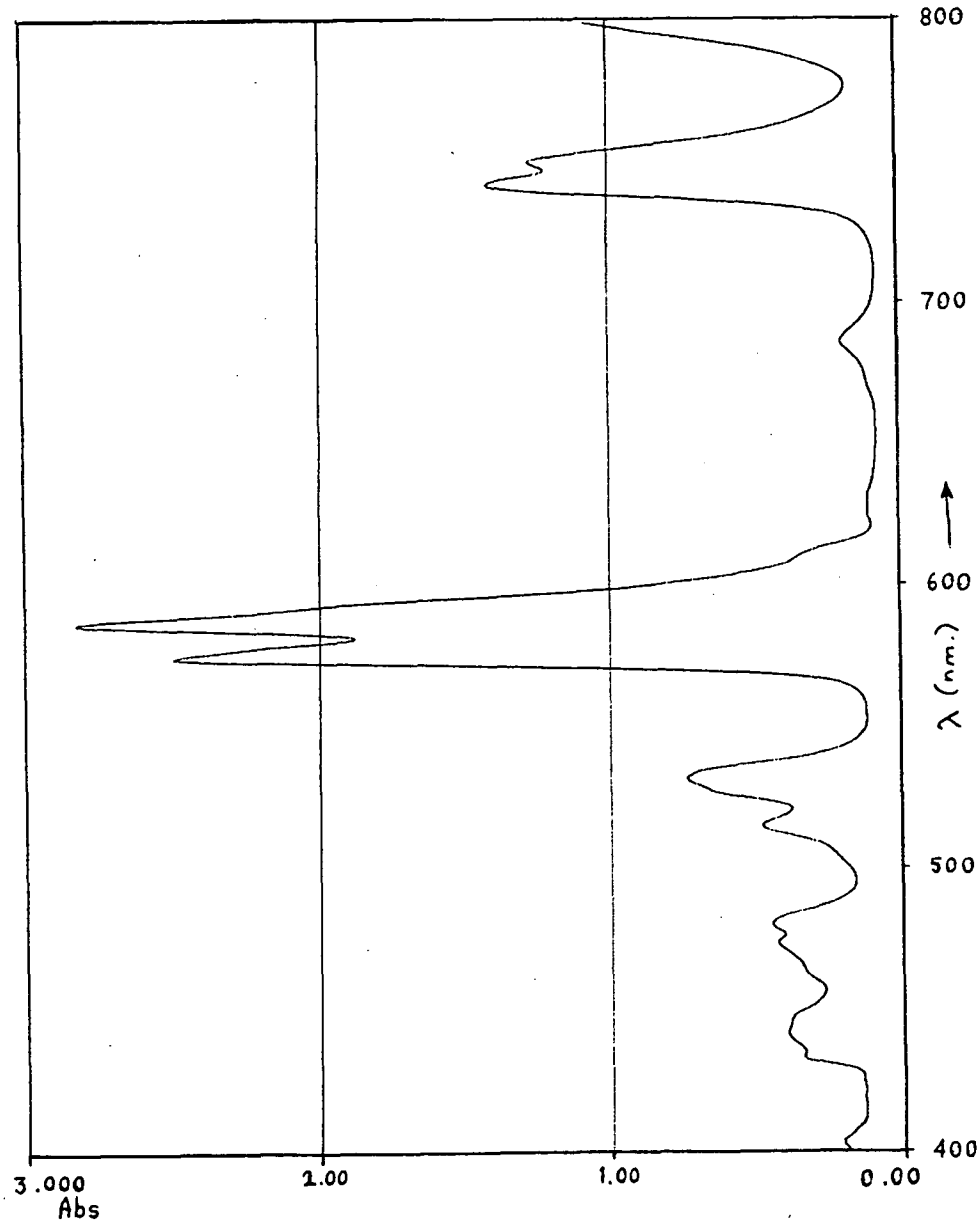

Figure 6-3: Absorption Spectrum of Neodymium Glass.

Conclusion

Various methods by which microscopic observations can be made more quantitative, rather than qualitative, have been discussed in this study. It is to be expected that this trend, which has so far been most evident with X-ray microanalysers and electron microscopes, will be more apparent in future with light-optical and accoustic microscopes as their electronic component becomes a more integral part of their design. The instruments of this type will not make the operator redundant however; quite the opposite can be expected : the advent of "intelligent" microscopes will enhance the quality of microscopic observations.

Two methods of digitising microscope images have been demonstrated and their limitations have been discussed. Television scanning has an inherently low level of aliasing error, due largely to the near-Gaussian electron-density profile of its reading beam. It suffers from a low signal-to-noise ratio and poor linearity however, particularly if a Vidicon tube is used. Microphotometric scanning has neither of these disadvantages and has a very good geometrical accuracy as well, but it is much slower. Its aliasing error can potentially be reduced by the aperture-modification indicated and there is great scope for improvement to the scanning speed by changes to the stepping-stage hardware.

The processes that follow image acquisition, those of image analysis, are directed towards an intelligent reduction of the very high amount of information present. The discussion in this study has been limited largely to a consideration of the analysis of images of tissue sections from biological specimens, admittedly a very common analysis problem. In many respects tissue sections are very awkward subjects for mathematical analysis since biological tissues have a wealth of detail down to and beyond the resolution limit of the light microscope.

As has been shown in Chapter 5 there are good statistical features for texture analysis when structural features are either absent or so variable as to be quite unreliable indicators. It is often advantageous to filter out visual information initially, as was done with the prostate tissue colouring, to assist in information reduction. Optical enhancement is also possible with histochemical staining of the tissues, and many aspects of these techniques remain to be evaluated. Is there, for example, some degradation of the textural statistics listed in Chapter 5 that can be shown to be due to the use of a non-Gaussian scanning aperture ? The role of colour-texture in portraying the pathological state of the tissue also remains to be studied; the tissue-stain used was a red/blue type while the illumination used was almost a spectral green.

There are thus limitations in image acquisition in image acquisition and optical analysis, which may be said to be problems of hardware, and there are many unexplored avenues of image analysis and data-reduction, which are essentially problems of the software. Of these two types of problems, it is the author's view that those relating to software are the furthest from adequate resolution. Advances in electro-optical imaging devices have made possible a very accurate recording of the light-microscope image; the subsequent treatment of this information in an attempt to mimic and surpass human comprehension with visual automata is still in its infancy.

APPENDIX 1 : Television Digitisation Programs

```
100 REM *** FRAME-GRABBER PROGRAM  "FRAG"
110
120 REM .... INITIALISATION
130 REM .... USER VIA - Port A = Output, Port B = Input
140 REM .... PB6=Composite SYNC    PB7=EOC from ADC _/=
150
155 *FX111,1
160 D%=178:?&79=D%:REM...No. of times each TV line is sampled
170 H%=4:?&78=H%:REM...Vert. jmp between samples
180 M%=&3000:?&7A=00:?&7B=&30:REM...Memory-base
190 N%=20:?&7C=N%:REM...No. of lines initially ignored
200 S%=128:?&7D=S%:REM...No. of TV lines sampled
205 I%=2:?&7E=I%:REM...Set interlace counter
310
320 DDRA=&FE63:DDRB=&FE62
330 PRTA=&FE61:PRTB=&FE60
340
350 FOR PASS=0 TO 3 STEP3
360 P%=&7200
370
380 [ OPT PASS
390 .GRAB
395 LDY #0
400 .INIT
410 LDA #&FF:STA DDRA  \ Set PRTA all outputs
420 LDA #&00:STA DDRB  \ Set PRTB all inputs
430 LDA &7D:STA &7F:LDA&7C:STA&77  \ temp-store for S% and N%
440 LDA #&7F:STA &FE4E:STA &FE6E  \ Disable all VIA interrupts
460
480 .PLOOP:LDA PRTB \ Wait for VSYNC event
490 ASL A:ASL A     \ c <-- PB6
500 BCS PLOOP
510 ASL &FFFF       \ 6 usec. delay
520 LDA PRTB        \ look for SYNC again
530 ASL A:ASL A
540 BCS PLOOP
542 DEC &7E:BNE PLOOP  \ Eliminate interlace
550 LDA &77:STA &7C  \ VSYNC found; set line-delay N%
555 LDA &7F:STA &7D  \ Set no. of lines sampled too
560 .PLUP:LDA PRTB  \ Wait for VSYNC to end
564 ASL A:ASL A:BCC PLUP
570
```

Program 'FRAG' (cont'd)

```
600 .SETHOR  \ Set up 74LS161's with current value of D%
610 LDA &79
620 STA PRTA
630
660 LDA #&40  \ Set bit6 of accum.
670 .DLOOP     \ Wait N% lines before looking at ADC
680 BIT PRTB
690 BNE DLOOP
700 DEC &7C  \ Decrement line-counter, N%
720 BNE DLOOP
730
780 .HLOOP  \ Wait for EOC of ZN448 on PB7
784 LDX &78
788 .HL
790 LDA PRTB:ASL A
800 BCC HL
802 DEX: BNE HL
810
820 .SNAP  \ Collect result from ADC and eject PB6
830 ASL A:LSR A:LSR A
840 STA (&7A),Y  \ and save it in memory
850 INC &7A:BNE FWRD  \ Increment mem.-pointer
860 INC &7B
870 .FWRD
880 DEC &7D   \ Decrement sample-counter S%
890 BNE HLOOP
900
910  LDA #&02:STA &7E \ Reset interlace counter
915 .SSTEP:DEC &79  \ Decrement line-sample counter D%
917 LDA&79:CMP#50
920 BNE PLOOP   \ Do next frame
930
940 LDA #&FF:STA &FE4E  \ Re-enable all interrupts
950 RTS
960
970 ]
980 NEXT
990
1000 CALL GRAB
2050 SOUND 1,-15,77,11
2060 CHAIN "UU"
3000 END
>
```

PROGRAM ' U ' : Rapid Display of TV scans

```
>L.
   40 !&2C90=&11011000
   44 !&2C94=&15051404
   46 !&2C98=&11011000
   48 !&2C9C=&15051404
   49 !&2CA0=&10100000
   50 !&2CA4=&11110101
   51 !&2CA8=&14140404
   52 !&2CAC=&15150505
   54  FOR N%=0 TO 255
   55 ?(&2B00+N%)=?(&2C90+N%DIV8)
   60 NEXT N%
   70 ?&8C=0:REM...COLOUR OFFSET
  100 MODE0
  105 *FX111,0
  110 REM...SCREEN / ARIES  DISPLAY
  120 OSBYTE=&FFF4
  140 FOR PASS=0 TO 2 STEP2
  144 P%=&C00
  150 [ OPT PASS
  200 .DIS
  204 LDA#&40:STA&84:LDA#&30:STA&85  \ Set top LHS of screen
  208 LDA#0:STA&8A:LDA#&30:STA&8B  \ set data base pntr
  212 LDA#&10:STA&8D  \ Set stripe cntr
  214 .LLP
  216 LDA#&6F:LDX#&81:JSR OSBYTE  \ turn on ARIES ram
  220 JSR BLOT
  224 LDA#&6F:LDX#&C0:JSR OSBYTE  \ turn off ARIES ram
  228 JSR GOB
  232 DEC&8D   \ see if all stripes done
  236 BNE LLP
  240 .FIN RTS
  280 .GOB
  400 .COL  \ S-R to put 1 block of bytes on to screen
  404 LDA#0:STA&86:STA&82:STA&87
  408 LDA#&0:STA&88:LDA#&2C:STA&89 \ set data pntr=&2C00
  412 LDA&84:STA&80:LDA&85:STA&81 \ Set screen pntr
  416 LDA#&4:STA&83  \ Set col cntr(3)=4
```

Program ' U ' (cont'd)

```
420 .SS
424 LDA#&20:STA&8F  \ Set cntr1=32
428 .RR
432 LDA#&04:STA&8E  \ Set cntr2=4
436 .QQ
440 LDY&86          \ collect data index
444 LDA(&88),Y:ADC&8C:TAX:LDA&2B00,X:ASLA \ make LHS nibble
448 STA&87:STY&86   \ save data & data index
452 TYA:CLC:ADC#&80:TAY \ add 128 to data index
456 LDA(&88),Y:ADC&8C:TAX:LDA&2B00,X \ make RHS nibble
460 ORA&87:INC&86   \ form scrn-byte & incr. data index
464 LDY&82  \ collect screen index
468 STA(&80),Y:INY  \ place byte on screen
472 STA(&80),Y:INY  \ & update scrn index
476 STY&82  \ save scrn index
480 DEC&8E  \ decr. cntr2 (4 times)
484 BNE QQ
488
492 LDY#0:STY&82  \ reset scrn index & keep data index
496 LDA&80:CLC:ADC#&80:STA&80  \ add 640 to scrn pntr
500 BCC BB:INC&81
504 .BB INC&81:INC&81
508 DEC&8F  \ decr. cntr1 (32 times)
512 BNE RR
516
520 INC&89  \ incr. data pntr by 256
524 LDA&84:CLC:ADC#&08:STA&84:STA&80  \ add 8 to top-scrn pntr
528 BCC DD:INC&85:LDA&85:STA&81  \ & reset (&80,&81)
532 .DD LDA&85:STA&81
536 LDA#0:STA&86  \ reset data index
540 DEC&83  \ decr. cntr3
550 BNE SS
560 RTS
670
680 .BLOT \ Block-transfer S-R
684 LDA#0:STA&88:LDA#&2C:STA&89 \ set target=&2C00
690 LDX#&04:LDY#&0
700 .LPA
710 LDA (&8A),Y:STA (&88),Y:INY
720 BNE LPA
730 INC &8B:INC &89:DEX
740 BNE LPA
750 RTS
760 ]
770 NEXT PASS
780 MODE2:CLG
800 CALL DIS
810 X=GET
820 ?&8C=?&8C+1
830 GOTO800
850 *FX111,1
900 END
```

APPENDIX 2 : Image-Analysis Programs

PROGRAM 'LAP'

```
>
>L.
  100 REM...Program for the analysis of anomalous Laplacian points
  110 REM...Scan data must be loaded at &3000 base-address
  120 PRINT "Screen must be in Mode 7"
  130 INPUT "Similarity-parameter",S%
  135 S%=S%*8
  140 N%=62:LL%=0:SS%=0:HH%=0
  150
  200 FOR M%=&3041 TO &3FBE
  220 GOSUB 600:REM...Form Neighbourhood values A% to J%, Ave. K%
  230 IF ABS(EE%-K%)<S% THEN 300
  235 LL%=LL%+1
  240 N%=N%-1
  250 IF N%=0 THEN GOSUB 800
  260 NEXT M%
  280 GOTO510
  300 REM...Detection and counting of saddle-points
  310 S1%=(D%+F%)-E%*2:S2%=(B%+H%)-E%*2
  314 IF (S1%*S2%)<-99 THEN 486
  320 S1%=(A%+J%)-E%*2:S2%=(C%+G%)-E%*2
  324 IF (S1%*S2%)<-99 THEN 486
  400 REM...Detection and counting of High-slope points
  410 A1%=ABS(E%-A%)+ABS(E%-B%)+ABS(E%-C%)+ABS(E%-D%)
  414 A2%=ABS(E%-F%)+ABS(E%-G%)+ABS(E%-H%)+ABS(E%-J%)
  418 A3%=A1%+A2%
  424 IF A3%>S% THEN HH%=HH%+1
  480 GOTO 490
  486 SS%=SS%+1
  490 N%=N%-1
  494 IF N%=0 THEN GOSUB 800
  500 NEXT M%
  510 REM...All required calculations finished
  520 PRINT "Fraction of Laplacian points is ";LL%/41
  524 PRINT "Fraction of Saddle points is ";SS%/41
  528 PRINT "Fraction of High-slope points is ";HH%/41
  555 END
  600 REM...Subroutine to form 3X3 neighbourhood values & (8*average)
  610 A%=?(M%-65):B%=?(M%-64):C%=?(M%-63)
  614 D%=?(M%-1):E%=?M%:F%=?(M%+1)
  618 G%=?(M%+63):H%=?(M%+64):J%=?(M%+65)
  620 K%=A%+B%+C%+D%+F%+G%+H%+J%
  624 EE%=E%*8
  630 REM...Do saddle-point tests
  699 RETURN
  800 REM...S-R To update line-counters
  810 N%=62:M%=M%+2
  820 RETURN
>
```

APPENDIX 2 : (cont'd)

PROGRAM 'GRAD'

```
>L.
  100 REM...Program for the counting of GRADIENT points
  110 REM...Scan data must be loaded at &3000 base-address
  120 PRINT "Screen must be in Mode 7"
  130 INPUT "Similarity-parameter",S%
  135
  140 GG%=0:N%=62
  150
  200 FOR M%=&3041 TO &3FBE
  220 GOSUB 600:REM...Form Neighbourhood values A% to J%, Ave. K%
  230
  240 X%=ABS(D%-F%):Y%=ABS(B%-H%)
  250 AA%=(X%+Y%)/2
  260 IF AA%>S% THEN GG%=GG%+1
  480
  490 N%=N%-1
  494 IF N%=0 THEN GOSUB 800
  500 NEXT M%
  510 REM...All required calculations finished
  520 PRINT "Fraction of Gradient points is ";GG%/41
  524
  555 END
  600 REM...Subroutine to form 3X3 neighbourhood values & (8*average)
  610 A%=?(M%-65):B%=?(M%-64):C%=?(M%-63)
  614 D%=?(M%-1):E%=?M%:F%=?(M%+1)
  618 G%=?(M%+63):H%=?(M%+64):J%=?(M%+65)
  624 EE%=E%*8
  630
  699 RETURN
  800 REM...S-R To update line-counters
  810 N%=62:M%=M%+2
  820 RETURN
>
```

APPENDIX 2 : (cont'd)

PROGRAM 'SOBEL'

```
>L.
  100REM...Program SOBel...15/3/85
  105 MODE7
  108 HIMEM=&3000
  120M%=&3081:R%=125
  130*FX 111,1
  135 FOR C%=1 TO 125
  140FOR K%=M% TO (M%+R%)
  150 *FX111,1
  160 D%=?K%:T1%=?(K%-1):T5%=?(K%+1)
  163 T3%=?(K%-&80):T7%=?(K%+&80)
  165 T2%=?(K%-&81):T6%=?(K%+&81)
  167 T4%=?(K%-&7F):T8%=?(K%+&7F)
  170 TH%=T2%+2*T3%+T4%
  174 TH%=(TH%-T8%-2*T7%-T6%)^2
  178 TF%=T4%+2*T5%+T6%
  180 TF%=(TF%-T2%-2*T1%-T8%)^2
  182 TS=SQR(TH%+TF%)
  184 D%=TS+0.5
  186  *FX 111,0
  188  ?K%=D%
  190NEXT K%
  200 M%=M%+&80
  220 NEXT C%
  230REM...All interior points done
  240 *FX 111,0
  244 FOR M%=&3000 TO &307F
  248  ?M%=?(M%+&80)
  252 NEXT M%
  256 FOR M%=&6F80 TO &6FFF
  260  ?M%=?(M%-&80)
  264 NEXT M%
  268 FOR M%=&3000 TO &6F80 STEP&80
  272  ?M%=?(M%+1)
  276  M%=M%+&7F
  278  ?M%=?(M%-1)
  280  M%=M%-&7F
  284 NEXT M%
  290 *FX 111,0
  300 *SAVE"S.XXXXXXXX" 3000 6FFF
  320 *FX 111,1
  330 SOUND 1,66,-15,5
  400 END
>
```

APPENDIX 2 : (cont'd)

PROGRAM 'BAT'

```
>L.
  100 REM...PROG. BHATTACHARYA
  102 M%=&7000
  104 REM...REQUIRES P200 @ &7000
  110 DIM SC(2,2)
  112 DIM SB(2,2)
  114 DIM S(2,2)
  116 DIM SI(2,2)
  118 DIM X(10,2)
  120 DIM Y(10,2)
  122 DIM XA(2)
  124 DIM YA(2)
  130 MSB%=0:LSB%=0
  200 INPUT "STATISTICS NOS.",R%,S%
  220 FOR I%=0 TO 9
  222 MSB%=?(M%+I%*20+(R%-1)*2)*256
  223 LSB%=?(M%+I%*20+(R%-1)*2+1)
  224 X(I%+1,1)=MSB%+LSB%
  226 MSB%=?(M%+I%*20+(S%-1)*2)*256
  227 LSB%=?(M%+I%*20+(S%-1)*2+1)
  228 X(I%+1,2)=MSB%+LSB%
  230 NEXT I%
  240 FOR I%=10 TO 19
  242 MSB%=?(M%+I%*20+(R%-1)*2)*256
  243 LSB%=?(M%+I%*20+(R%-1)*2+1)
  244 Y(I%-9,1)=MSB%+LSB%
  246 MSB%=?(M%+I%*20+(S%-1)*2)*256
  247 LSB%=?(M%+I%*20+(S%-1)*2+1)
  248 Y(I%-9,2)=MSB%+LSB%
  250 NEXT I%
  255
  260 REM...CALCULATE AVERAGES XA,YA
  261 XA(1)=0:YA(1)=0:XA(2)=0:YA(2)=0
  262 FOR I%=1 TO 10
  264  XA(1)=XA(1)+X(I%,1)
  266  XA(2)=XA(2)+X(I%,2)
  268  YA(1)=YA(1)+Y(I%,1)
  270  YA(2)=YA(2)+Y(I%,2)
  272 NEXT I%
  274 XA(1)=XA(1)/10:XA(2)=XA(2)/10
  276 YA(1)=YA(1)/10:YA(2)=YA(2)/10
```

PROGRAM 'BAT' (cont'd)

```
300 REM...FORM Sx AND Sy (Sc & Sb)
320 FOR I%=1 TO 10
330  SC(1,1)=SC(1,1)+X(I%,1)*X(I%,1)
332  SC(1,2)=SC(1,2)+X(I%,1)*X(I%,2)
334  SC(2,1)=SC(2,1)+X(I%,2)*X(I%,1)
336  SC(2,2)=SC(2,2)+X(I%,2)*X(I%,2)
340  SB(1,1)=SB(1,1)+Y(I%,1)*Y(I%,1)
342  SB(1,2)=SB(1,2)+Y(I%,1)*Y(I%,2)
344  SB(2,1)=SB(2,1)+Y(I%,2)*Y(I%,1)
346  SB(2,2)=SB(2,2)+Y(I%,2)*Y(I%,2)
350 NEXT I%
352 SC(1,1)=SC(1,1)-10*XA(1)*XA(1)
354 SC(1,2)=SC(1,2)-10*XA(1)*XA(2)
356 SC(2,1)=SC(2,1)-10*XA(2)*XA(1)
358 SC(2,2)=SC(2,2)-10*XA(2)*XA(2)
362 SB(1,1)=SB(1,1)-10*YA(1)*YA(1)
364 SB(1,2)=SB(1,2)-10*YA(1)*YA(2)
366 SB(2,1)=SB(2,1)-10*YA(2)*YA(1)
368 SB(2,2)=SB(2,2)-10*YA(2)*YA(2)
370
372 REM...FORM POOLED COVAR. MATRIX
374 S(1,1)=(SC(1,1)+SB(1,1))/36
376 S(1,2)=(SC(1,2)+SB(1,2))/36
378 S(2,1)=(SC(2,1)+SB(2,1))/36
380 S(2,2)=(SC(2,2)+SB(2,2))/36
390 REM...INVERT P.C.MATRIX
392 D=S(1,1)*S(2,2)-S(1,2)*S(2,1)
394 SI(1,1)=S(2,2)/D
395 SI(1,2)=(-1)*S(1,2)/D
396 SI(2,1)=(-1)*S(2,1)/D
397 SI(2,2)=S(1,1)/D
400
410 REM...CALC. DISCRIMINANT Drs
420 M1=YA(1)-XA(1)
422 M2=YA(2)-XA(2)
430 D1=M1*M1*SI(1,1):D2=M1*M2*SI(2,1)
434 D3=M2*M1*SI(1,2):D4=M2*M2*SI(2,2)
436 Drs=5*(D1+D2+D3+D4)
500 PRINT Drs
999 END
```

Appendix 3 : Program 'SPAA'

```
>L.
  10 REM...PROGRAM SPAA (SPECTRA COLLECTION)
  20 REM TURN ON CHANNELS 1,2 & 3
  25 ?&FE61=&FF
  30 *FX16,3
  40  DIM A(220):REM...Calib'n. pts
  50  DIM B(220):REM...Transm. pts
  60  DIM L(220):REM...Lambda array
  70 REM....Go to 400 nm. pos'n.
  80 GOSUB 950
  90 REM SPECTRA-PLOTTER
 100 GOSUB 770:REM GRAFICS SETUP
 110 REM TAKE CALIBRATION SPECTRUM
 120 LAMBDA=158+(ADVAL(3)/70.74)
 130 L(CN%)=LAMBDA
 140 LL%=LAMBDA*2.72-928
 150 REM PLOT AND STORE RESULT
 160 GOSUB 470
 170 REM TAKE Q STEPS
 180 GOSUB 700
 190 IF LL%<1260 AND LL%>0 THEN 120
 200 REM Calib. done...Go To 530nm.
 210 L1%=530:GOSUB970
 220 REM....Start of Transm. Spec.
 230 MOVE 200,240
 240 INPUT "Ready for Analysis",AA
 250 GOSUB 770
 260 GOSUB 950:REM Go to 400nm.
 270 LAMBDA=158+(ADVAL(3)/70.74)
 280 LL%=LAMBDA*2.72-928
 290 REM PLOT Normalised Transmission
 300 GOSUB 540
 310 REM TAKE Q STEPS
 320 GOSUB 700
 330 IF LL%<1260 AND LL%>0 THEN 270
 340 REM SPEC finished...Go To 530nm.
 350 L1%=530:GOSUB970
 360 MOVE 300,24
 370 REM....Spectrum-Printout ?
 380 INPUT "Printout required",A$
 390 IF LEFT$(A$,1)<>"Y" THEN 230
 400 GOSUB 1250:REM...Turn on TTY
 410 GOSUB 640:REM....Print-out
 420 GOSUB 1320:REM...Turn off TTY
 430 REM.....Continue if desired
 440 GOTO 230
 450 VDU4
 460 END
```

```
470 REM S-R TO TAKE CALIBRATION SPEC.
480 FOR N=1 TO 10
490  A(CN%)=A(CN%)+ADVAL(1)/16
500 NEXT N
510 A(CN%)=A(CN%)/10
520 PLOT 5,LL%,A(CN%)/2
530 RETURN
540 REM S-R TO PLOT TRANSMISSION SPEC.
550 RD%=0
560 FOR N=1 TO 4
570 RD%=RD%+ADVAL(1)
580 NEXT N
590 TR%=(RD%*15/A(CN%))
600 IF TR%>960 THEN TR%=960
610 B(CN%)=TR%/9.6
620 PLOT 5,LL%,TR%
630 RETURN
640 REM...S-R to print results to TTY
650 FOR C%=0 TO 204 STEP 4
660     B%=B(C%)+10.5
670   PRINT L(C%);TAB(B%);"*"
680 NEXT C%
690 RETURN
700 REM S-R TO MOVE Q STEPS
710 CN%=CN%+1
720 REM nm. step-scaling factor
730 FOR Q=1 TO 2
740 GOSUB 1080
750 NEXT Q
760 RETURN
770 REM INITIALISE GRAFICS
780 MODE4
790 VDU19,0,4,0,0,0
800 VDU19,1,6,0,0,0
810 CLG
820 VDU5
830 FOR X%=1248 TO 160 STEP-272
840 MOVE X%,960
850 DRAW X%,0
860 NEXT X%
870 FOR X%=0 TO 1088 STEP272
880 MOVE (X%-132),1000
890 PRINT (400+(X%*100/272))
900 NEXT X%
910 MOVE160,0
920 RD%=0
930 CN%=0
940 RETURN
950 REM S-R TO AUTO-SEEK START W/L
```

```
950 REM S-R TO AUTO-SEEK START W/L
960 L1%=400
970 L2%=158+ADVAL(3)/70.74
980 IF ABS(L1%-L2%)<1 THEN 1060
990 IF (L1%-L2%)>0 THEN 1030
1000 REM NEGATIVE STEP
1010 GOSUB1180:GOSUB1080:GOSUB1180
1020 GOTO 970
1030 REM POSITIVE STEP
1040 GOSUB1080
1050 GOTO 970
1060 SOUND 1,-15,120,6
1070 RETURN
1080 REM STPG MOTOR SUBROUTINES
1090 REM SUBROUTINE STEX
1100 Q%=?&FE61
1110 Q%=Q%-2:?&FE61=Q%
1120 FOR T=1 TO 15
1130 NEXT T
1140 Q%=Q%+2:?&FE61=Q%
1150 FOR T=1 TO 85
1160 NEXT T
1170 RETURN
1180 REM SUBRTNE INVX
1190 Q%=?&FE61
1200 IF Q%>127 THEN 1230
1210 Q%=Q%+128:?&FE61=Q%
1220 RETURN
1230 Q%=Q%-128:?&FE61=Q%
1240 RETURN
1250 REM...S-R to turn on TTY
1260 *FX5,2
1270 *FX6,0
1280 *FX8,3
1290  VDU2
1300  VDU21
1310 RETURN
1320 REM...S-R to turn off TTY
1330 VDU6
1340 VDU3
1350 RETURN
```

REFERENCES

1.1: Hall,E.L.: Computer Image Processing and Recognition, Chapter 7, Academic Press, New York, 1979.

1.2: Russ,J.C. and Russ,J.C.: Image Processing in a General Purpose Microcomputer, Journal of Microscopy, Vol.135,pp.89-102, July 1984.

2.1: Sandritter,W. and Kiefer,G.: Methoden und Ergebnisse der Zytophotometrie und Interferenzmikroskopie, Acta Histochemica (Jena), Suppl. IV, 1965.

2.2: Zimmer,H.: Microphotometry, from: Molecular Biology, Biochemistry and Biophysics, Vol.14, p.304, Springer-Verlag, Berlin, 1973.

2.3: Eastgate,A.R.: Research Report 1981-1983, Physics Department,p.C01, University of Tasmania, 1983.

2.4: Mertz,P. and Gray,F.: Bell Systems Technical Journal, Vol.13, p.464, 1934.

2.5: Duda,R.O. and Hart,P.E.: Pattern Classification and Scene Analysis, Chapter 8, pp.302-305, Wiley and Sons, New York, 1973.

2.6: Goodman,J.W.: Introduction to Fourier Optics, Chapter 6, pp.120-125 McGraw-Hill, New York, 1968.

2.7: Huck,F.O., Halyo,N. and Park,S.K.: Aliasing and Blurring in 2-D Sampled Imagery, Applied Optics, Vol.19, pp.2174-2181, July 1980.

2.8: Katzberg,S.J., Huck,F.O. and Wall,S.D.: Applied Optics, Vol.12, p.1054, 1973.

3.1: Grob,B.: Basic Television, 4th Edn., Chap.5, p.68, McGraw-Hill, Kogakusha, 1976.

3.2: Rosenfeld,A.: UMIPS Manual, Computer Vision Laboratory Publication, University of Maryland, 1984.

3.3: Eastgate,A.R.: Research Report 1981-1983, p.C7, Physics Department, University of Tasmania 1983.

4.1: Arfken,G.: Mathematical Methods for Physicists, Academic Press, New York, 1968.

4.2: Weszka,J.S. and Rosenfeld,A.: Histogram Modification for Threshold Selection, IEEE Trans. on Systems, Man and Cybernetics, Vol. SMC-9, No.1, January 1979.

4.3: Lytton,D.G., Eastgate,A.R. and Ashbolt,N.J.: Digital Mapping of Metal-bearing Amoebocytes in Tissue Sections of the Pacific Oyster, Journal of Microscopy, No.138, pp.1-14, April 1985.

4.4: Eastgate,A.R.: Research Report 1981-1983, p.C11, Physics Department, University of Tasmania, 1983.

4.5: Peleg,S.: Iterative Histogram Modification, IEEE Trans. on Systems, Man and Cybernetics, Vol.SMC-8, pp.555-556, 1978.

4.6: Bhanu,O. and Faugeras,O.D.: Segmentation of Images Having Unimodal Distributions, IEEE Trans. on Pattern Analysis and Machine Intelligence Vol.PAMI-4, No.4, pp.408-419, July 1982.

4.7: Rosenfeld,A. and Weszka,J.S.: Texture Analysis, in Digital Pattern Recognition, Ed. by K.S.Fu, Ch.5, p.146, Springer-Verlag, Berlin 1976.

4.8: Duda,R.O. and Hart,P.E.: Pattern Classification and Scene Analysis, Chap.7, pp.271-273, Wiley-Interscience 1973.

5.1: Zucker,S.W.: Toward a Model of Texture, Computer Graphics and Image Processing (CGIP), Vol.5, pp.190-202, (1976).

5.2: Haralick,R.M.: Statistical and Structural Approaches to Texture, Proc. of the IEEE, Vol.67, No.5, pp.786-804, (1979).

5.3: Ballard,D.H. and Brown,C.M.: Computer Vision, Chap.6, pp.166-194, Prentice-Hall, 1982.

5.4: Julesz,B.: Visual Pattern Discrimination, IRE Trans. on Information Theory, Vol.IT-8, pp.84-92, February 1962.

5.5: Fu,K.S.: Digital Pattern Recognition, Chapter 3, Springer-Verlag, New York, 2nd Edition, 1980.

5.6: Brodatz,P.: Textures - A Photographic Album for Artists and Designers, Dover, New York, 1956.

5.7: Pratt,W.K., Faugeras,O.D. and Gagalowicz,A.: Visual Discrimination of Stochastic Texture Fields, IEEE Trans. Syst., Man, Cybern., November 1978.

5.8: Faugeras,O.D. and Pratt,W.K.: Decorrelation Methods of Texture Feature Extraction, IEEE Trans. Patt. Anal. and Machine Intelligence, July 1980.

5.9: Li,C.C. and Fu,K.S.: Machine Classification in Medicine, in Annual Review of Biophysics and Bioengineering, Vol.9, Ch.14, p.405, (1980).

5.10: Diday,E. and Simon,J.C.: Clustering Analysis, in Digital Pattern Recognition, Ed. by K.S.Fu, Chap.3, p.89, Springer-Verlag, Berlin, 1980.

5.11: Abdou,I.E. and Pratt,W.K.: Quantitative Design and Evaluation of Enhancement/Thresholding Edge Detectors, Proc. of the IEEE, Vol.67, No.5, pp.753-763, May 1979.

5.12: Zehna,P.W.: Introductory Statistics, Chap.9, Prindle Weber and Schmidt Inc., Boston, Massachusetts, 1974.

6.1: James,J.F. and Sternberg,R.S.: The Design of Optical Spectrometers, Chap.1, p.12, Chapman and Hall Ltd., London 1969.

6.2: Burns,R.G.: Mineralogical Applications of Crystal Field Theory, Chap.3, Cambridge Earth Science Series, Cambridge University Press, London 1970.

6.3: Kingslake,R.: Optical System Design, Chap.16, p.310, McGraw-Hill, New York 1983.

6.4: Brain,T., Eastgate,A.R. and Lytton,D.G.: Spectral Studies of Haematoxylin/Eosin Staining, Proc. of Royal Aust. College of Pathologists Scientific Meeting, Perth, October 1984.